DISSERTATION

MODELING THE SPATIAL AND TEMPORAL DYNAMICS OF THE AMBER-MARKED BIRCH LEAF MINER INFESTATION IN ANCHORAGE, ALASKA

Submitted by

Michael Francis Tuffly

Department of Forest and Rangeland Stewardship

In partial fulfillment of the requirements

For the Degree of Doctor of Philosophy

Colorado State University

Fort Collins, Colorado

Fall 2012

Doctoral Committee:

Advisor: Robin Reich

William Jacobi
Rajiv Khosla
John Lundquist

ABSTRACT

MODELING THE SPATIAL AND TEMPORAL DYNAMICS OF THE AMBER-MARKED BIRCH LEAF MINER INFESTATION IN ANCHORAGE, ALASKA

Since 1998, the invasive insect amber-marked birch leaf miner (*Profenusa thomsoni* Konow.) has been an issue for the birch trees in Alaska's Anchorage Bowl. *P. thomsoni* is native to Europe and an invasive defoliator of birch trees; its impacts are considered aesthetically unpleasing to Anchorage residents. In this study, a spatial and temporal model was constructed using a cellular automata (CA) method. Employing the statistical program R (R Development Core Team 2008), coupled with a custom library called RandomFields (Schlather 2012) and linear regression techniques, a CA model was created. Using five years of field data gathered between 2006 and 2010 (Lundquist et al. 2012), the CA model mimics the observed change in severity of the infestation based upon the severity in the previous year and if the region was in an area that increased or decreased in severity. A voracity test was used to compare the CA model output for the time period of the observed field data; a sensitivity analysis on various input parameters was also implemented. The CA model simulated results were analyzed for the time period 1998 to 2018 and indicated that *P. thomsoni* may follow three primary phases: 1) expansion, 2) decline, and 3) equilibrium. The expansion phase demonstrated a six-year spatial spread cycle, which can be described as random, disjointed regions of high infestation that move about the landscape. The expansion phase may be the result of an abundance of host, lack of natural enemies, and no density-dependent factors. The declining phase is depicted as a decrease in severity at an increase rate. The declining phase is possibly due to the combination of density-dependent factors and natural enemies. The equilibrium phase is a possible product of long-term plant defenses. The development of this spatial and temporal predictive CA model will allow resource managers to be proactive in order to mitigate and manage the *P. thomsoni* infestation. In

addition, this modeling method can be used to simulate other forest pests and pathogens at the landscape level.

ACKNOWLEDGEMENTS

The learning process needed for a doctoral degree is vast and complex. Therefore, I would like to thank Dr. Robin Reich for his guidance, support, and patients. Next, I would like to thank Dr. John Lundquist for his advice and valuable input. I would like to thank my wife Melannie Hartman for her tolerances and assistance during the writing of this document. Finally, and foremost I would like to thank my brother Robert Tuffly for his time and effort editing this document.

DEDICATION

I dedicate this document to the memory of Dr. Bart Tuffly (1928 – 2000).

TABLE OF CONTENTS

LIST OF FIGURES

LIST OF TABLES

INTRODUCTION

Outbreaks of the amber-marked birch leaf miner (*Profenusa thomsoni* Konow.), an invasive forest insect from Europe, has infested the urban birch forest of Anchorage, Alaska (Goldstein et al. 2005). It is believed *P. thomsoni* was first introduced into North America (New England) circa 1920 (Benson 1959, Soper et al. 2009, MacQuarrie et al. 2010). This introduction is likely the result of humans transporting live, infested birch trees from Europe (Digweed and Langor 2004). *P. thomsoni* subsequently infested Vermont, Massachusetts and Maine, as well as most provinces and territories in Canada (Quebec, Manitoba, and Northwest Territories) (Soper et al. 2009). In the 1970s, *P. thomsoni* (Digweed and Langor 2004*)* was discovered in the Canadian province of Saskatchewan. *P. thomsoni* was first confirmed in Anchorage, Alaska, in 1996 (Snyder et al. 2007). Since 2006, two additional invasive sawflies that caused considerable damage to birch trees were identified in Anchorage: 1) the late birch leaf edge miner (*Heterarthrus nemoratus* Fallén.), and 2) the birch leaf miner (*Fenusa pumila* Leach.).

P. thomsoni is a defoliator and feeds exclusively on birch trees (*Betula* spp.). It is native to Europe where it does not present a threat to the birch forest (Digweed et al. 2003). The low population levels of *P. thomsoni* in European forests are thought to be caused by indirect competition for resources with other sawflies (*F. pumila* or *H. nemoratus*) and predation (Digweed 2006).

P. thomsoni is univoltine (MacQuarrie et al. 2010). The insect overwinters in the forest duff as prepupae, which emerge in late May to early July when leaves form on birch trees. However, depending on temperature and humidity, adult insects continue to emerge for most of the summer. Adults are 0.31 to 0.63 cm long, black in color, and are almost always females. Oviposition peaks in late June. The larvae that emerge from eggs after 12 days feed on the leaf tissue between the epidermal layers, forming blotch mines that enlarge as sawfly larvae

develop, often coalescing when larvae are crowded (Digweed et al. 2009). The larvae pass through six instars, the last of which cuts a hole in the leaf, drops to the litter below, burls into the duff, and pupates (Digweed et al. 2009). Impacts to trees are limited primarily to decreased aesthetic values due to browning, distortion, or premature loss of foliage. For a detailed description of the *P. thomsoni* life cycle, see Snyder et al. (2007) or MacQuarrie et al. (2010).

Lundquist et al. (2012) describes the spatial and temporal dynamics of the *P. thomsoni* infestation in Anchorage as a patchy landscape pattern. Over time, it has been observed that areas of increased infestation levels move about the landscape in the form of disjoint regions, encompassing the entire city of Anchorage in approximately six years. A similar spatial pattern was described by Petrovskii et al. (2002) in a predator-prey environment.

Modeling the temporal and spatial movements of insect invasion over the landscape can be a complex and a time-consuming process (Sharov 1996). At the beginning of most invasion some kind of population front is formed (Petrovskii et al. 2002). The spread of the invasion over the landscape may form into a wave- like pattern (Yemshanov et al. 2009) or be sculpted by predators into irregular patches (Petrovskii et al. 2002). Many types of invasion waves are described in the literature. Some examples of these waves are: 1) a simple traveling wave front (Huang et al. 2008), 2) oscillating wave (Liebhold and Kamata 2000, Haynes et al. 2009), and 3) a reaction-diffusion wave (Fisher 1937, Schofield 2002, Richter et al. 2012). Each of these wave types has some similarities and differences that involve different levels of modeling efforts.

A simple traveling wave front is the simplest form of spread across the landscape where insects originating from an infestation point or region spread into new areas in all directions in a linear pattern at a uniform rate (e.g. 1km/year). Often, many infestation points or foci occur simultaneously in a traveling wave front. The infestation points radiate outward, eventually coalescing into a single wave front that travels across the landscape at relatively

uniform rates as a single unit. Due to the uniformity of spread rates and patterns, the traveling wave front is one of the simplest to model.

An oscillating wave front is similar to the simple traveling wave front, except for some temporal and spatial variations in spread rate that can be influenced by many factors. For example, bivoltine insects have a two-year temporal oscillation in population numbers. Liebhold and Kamata (2000) term this as periodic oscillating. Also, some insects prefer host trees under stress due to drought or disease (Mercader et al. 2011). These stressed trees are often dispersed throughout the forests in a patchy landscape, producing a spatial variation in insect infestation. Finally, temporal and spatial oscillation may occur in tandem. Case in point, temperature is an influential factor on insect fecundancy. Increases in average annual temperatures may cause some insects to transition from bivoltine to univoltine. In addition, under drought conditions temperature is often increased, which can influence both spatial and temporal variations and produce an oscillating wave front. Because of the above factors, modeling an oscillating wave front adds an additional layer of complexity when compared to the simple traveling wave front. The application of trigonometric functions in the construction of these type of spread models can be used to capture the temporal oscillation. Spatial data depicting the distribution or quality of host species may address the spatial variability (Morin et al. 2009).

A reaction-diffusion wave is different from the simple or oscillating wave because of the application of differential equations to solve for non-linear spread rates (Richter et al. 2012). Some factors that may drive the non-linear spread rates are fecundancy and environmental. One of the first reaction-diffusion equations was developed by Fisher (1937) in his work on favorable mutations on advantageous gene and how these gene were distribute in a population. Another component that can be accounted for in the reaction-diffusion model is the Allee effect (Allee 1927, Petrovskii et al. 2002, Schofield 2002, Taylor and Hastings 2005, Liebhold and Tobin 2008, Richter et al. 2012), which has been described as some critical lower

population value at which the insect population must be above to remain viable and spreading (Liebhold and Tobin 2008). Due to the potential number of environmental factors coupled with the differential equations, the reaction-diffusion spread models are some of the most complex and difficult to create.

The *P. thomsoni* infestation in Anchorage does not mirror any of the typical wave type invasions. This infestation produces groups of trees that illustrate cyclic eruptions in severity. These cyclic eruptions vary in size, shape and intensity and are randomly move over the landscape. A similar type of landscape infestation is described by Petrovskii et al. (2002). Petrovskii et al. (2002) describes an invasion front breaking up into separate irregular patches over the landscape in a predator-prey system.

Early insect spread models used the following equation (Varley et al. 1973)

$$N_t = N_0 e^{rt} \qquad [1]$$

where N_t is the number of individuals at time t and r is the intrinsic rate of growth (i.e. birth rate – death rate), with no consideration of carrying capacity and assumes the spread was isotropic in nature. Other insect spread models use historical data coupled with ancillary variables (e.g. temperature or host distribution) to create spread models (Liebhold et al. 1992). It appears that many spread models follow a general stochastic approach (Rasmussen and Hamilton 2012). A simple stochastic spread model could take the form of a series of variables, with random values funneled into some mathematical function and simulated hundreds of times to produce an outcome. Summary statistics (e.g. mean, maximum, and variance) from these simulations can be assessed and compared to observed data.

Hartley et al. (2010) succeeded in predicting suitable habitat for Argentine ants (*Linepithema humile* Mayr.) in Hawaii using a single variable (i.e. temperature) in the form of degree days, coupled with a Geographic Information System (GIS). Climate can impact potential habitats by simultaneously affecting host and insect population dynamics by directly

killing the pest due to temperature extremes or indirectly by influencing host phenology and general tree health (Liebhold et al. 1992).

DeRose and Long (2012) used a general linear model (glm) to identify the factors driving Englemann spruce (*Picea englemannii* Parry ex Engelm.) mortality in Utah due to the spruce beetle (*Dendroctonus rufipennis* Kirby.) infestation. Focusing their attention on the host, they found that slope, tree diameter, tree density, and forest stand structure coupled with ancillary environmental factors identified susceptible forest stands. DeRose and Long (2012) illustrated that spruce beetle spread did not originate from a single epicenter; rather, it spread in a simple wave-like pattern across the landscape. They concluded that the decline in the spruce beetle population was the result of host depletion.

Complex stochastic models have been used to evaluate the spread of invasive insects. Mercader et al. (2009) for example, measured the dispersal rate over one generation of emerald ash borer *(Agrilus planipennis* Fairmaier.). These data were then fitted to a negative exponential function. Results of this experiment showed that insects dispersed 100 m per year from infested trees in all directions.

Many spread models make the assumption that if the host is uniformly distributed across the landscape, then the spread will also be uniform. Morin et al. (2009) investigated the directional spread of hemlock wooly adelgid (*Adelges tsugae* Annand.) in the eastern United States from 1951 to 2006. Results indicated that the spread was anisotropic due to the variability in climate and the abundance of host species. In addition, the magnitude of anisotropy varied over time.

Yemshanov et al. (2009) used a stochastic process to model the introduction and spread of an invasive wood wasp (*Sirex noctilio* Fabricius.) in the eastern United States and Canada. They modeled the probability that an introduction of the wasp could occur based upon the amount of cargo a particular area was receiving and if that cargo originated from countries where the wood wasp resided. Using host distribution data Yemshanov et al. (2009) generated

a series of scenarios to illustrate where and how fast the infestation would occur coupled with a level of uncertainty.

Schofield (2002) investigated the use of reaction-diffusion equations to model the spatial-temporal spread of a parasite (*Wolbachia*) infecting the fruit fly (*Drosophila simulans*) population in California. This stochastic model produced results termed as a traveling wave invasion. A key finding indicated that a minimum density value of infected fruit flies was required to sustain a traveling wave invasion of parasites in the population. However, this wave invasion may reverse (decline) if, and only if, the population of infection fruit flies reaches some critical lower population level. The parasite will become locally extinct if the number of infected fruit flies drops below some critical minimum density (i.e. Allee effect).

Recently, the use of network models for predicting spread of infectious diseases are showing promise, particularly in systems where anthropogenic transportation vectors are plentiful (Bian and Liebner 2005, Jeger et al. 2007). Network models or neural networks are an artificial means to emulate the decision system in the human brain. The network consists of three main layers: input layers, hidden layers, and output layers. At the transition to a new layer are nodes where decisions are made. The decisions are a Boolean function and are stored in the hidden layer that can be trained by the user. As input data are fed into the model, the outputs are inspected by the user. The results of the output are fed back to the hidden layer, illustrating a correct or incorrect answer. The hidden layer learns by this feedback from the user, thereby becoming "intelligent" and capable of making independent decisions. Some authors have termed this process as artificial intelligence (Perez and Dragicevic 2012). Therefore, no decision rules per se are required by the user (Atkinson and Tatnall 1997).

Most of the current research in neural networks is focused on the spread of infectious disease in animals (Jeger et al. 2007) and the classification of remotely sensed data. Some specific examples of network models are: food webs, electrical power grids, and the spread of diseases in animal populations (Jeger et al. 2007). These network examples use input layers

depicting organisms, power generating stations, or infected individuals, respectively. The hidden layer stores the decision-making components that subsequently comprise the output layer and answers the questions of who is going to be consumed, where the power will go, and who will become ill. In addition, these network examples are directional: 1) heterotrophic animals eat autotrophic animals, 2) power moves from where it is generated to where it is consumed, and 3) healthy animals become ill by coming in contact with infected animals.

Agent-Base Models (ABM) or multi-agent systems are another class of models that has been used to model spread and outcomes of many natural and anthropogenic situations (Chan et al. 2010, Perez and Dragicevic 2012). For example, ABM has been employed to model the spread of infectious disease in humans, wildfire spread (Bauer et al. 2009), and for decision making under landuse change scenarios (Deadman et al. 2004). ABM contains three main components: 1) agents, 2) rules that drive the agents, and 3) interactions between agents via the rules (Sudhira et al. 2005). The agents are a set of autonomous objects such as trees or animals, and have the ability to learn via artificial intelligence (Sudhira et al. 2005, Perez and Dragicevic 2012), analogous to the hidden layer in the neural networks model. The rules and interactions are often encapsulated into one element or process.

These rules and interactions that drive the agents are pre-defined and can be simple or complex. Chan et al. (2010) discuss the Boids (bird-like objects) (Reynolds 1987) ABM, which simulates flocking behavior in birds or schooling behavior in fish. The Boids ABM uses either fish or birds as agents and has three simple rules and interactions: 1) Separation: steer to avoid crowding local individuals, 2) Alignment: steer towards the average heading of local individuals, and 3) Cohesion: steer towards the average position of local individuals. The Boids model starts with a finite set of agents (e.g. fish or birds) randomly distributed in finite space and simulated in discreet steps thousands of times. The results of Boids model simulation produces groups or clusters of agents over the finite space (Chan et al. 2010). ABM

is also considered a bottom-up modeling method (Sudhira et al. 2005, Perez and Dragicevic 2012), which means the smallest element (agent) drives the final outcome.

Cellular automata (CA) is another modeling method used to model the spread of organisms over the landscape (Campos et al. 2008, Huang et al. 2008, Mathey et al. 2008, Chan et al. 2010, Perez and Dragicevic 2012, Rasmussen and Hamilton 2012). Introduced by von Neumann (1951), the CA model has been described as a mathematical model consisting of simple and identical components that act together to form a complex behavior (Han et al. 2012). Zhou and Liebhold (1995) offer additional context for the CA definition: "a model acting upon a multi-dimensional matrix of cells, a cell may exists in only one possible state at a discrete time period, cell states are updated at every time step via simulation." CA is considered a bottom up modeling technique in which cells make neighborhoods, rules change neighborhoods in discrete time steps, and cells interact with rules and neighborhoods (Perez and Dragicevic 2012).

CA contains three main components: 1) the cell or lattice as the primarily modeling element, 2) a finite number of cells comprising a neighborhood of cells, and 3) cell transition rules (Sudhira et al. 2005, Huang et al. 2008). A cell can be a soil type, forest cover type, or animal population values. A simple example of a CA model is Conway's game of life model (Berlekamp et al. 2003), where a set of finite number of cells are randomly distributed across the landscape and have one, and only one, of two states (i.e. alive or dead). Each cell changes its state at each discrete time step based upon three rules: 1) a live cell with at least three live adjacent neighbors will remain alive in the next time step, 2) a dead cell with at least three live adjacent neighbor will come to life in the next time step, and 3) if rule number 1 and 2 are false, then the cell dies in the next time step (Chan et al. 2010). The results from thousands of simulations of Conway's game of life produces a diverse set of aggregated cells (neighborhoods) based upon their state.

Zhou and Liebhold (1995) used CA in modeling the spatial dynamics of gypsy moths (*Lymantria dispar* L.) in Massachusetts. Input data was gathered from historical maps (1961 – 1991), depicting the movement of gypsy moths across the landscape. The CA models were tested using eight different rules (transitional states): 1) simple Markov chain, 2) rook's move, 3) queen's move, 4) weighted means, 5) weighted means in susceptible areas, 6) weighted means with frequency models, 7) weighted means with egg mass counts, and 8) weighted means with egg counts and only in susceptible areas. In conclusion, models 6, 7, and 8 (above) closely followed the observed data.

CA and ABM share some general commonalities (Sudhira et al. 2005, Chan et al. 2010, Perez and Dragicevic 2012), which are: 1) stochastic in nature, 2) spatially explicit, 3) depicting spread or movement over time, 4) modeling of an individual entity (e.g. a cell or agent), 5) bottom up modeling and 6) following user defined rules. Both CA and ABM also require a programming language (e.g. C^{++}, Python, or R), a mathematical algorithm, methodology, and rules. In contrast, CA and ABM differ on three key elements. CA uses cells and neighborhoods, whereas ABM uses agents. CA implements an action on all the cells at a single time step, while ABM can selectively act upon individual agents at differ time periods. Finally, CA cells are not autonomous, while ABM agents are (Sudhira et al. 2005, Chan et al. 2010).

As a general rule, ABM is more complex than CA due to the ability to selectively act upon individual agents, at different time periods, coupled with the agent autonomy (Sudhira et al. 2005, Perez and Dragicevic 2012). ABM has not been widely applied to modeling the spread of forest pests because many agents and interactions of a pest invasion are poorly understood, which creates a significant challenge when attempting to assemble data and programming the model. In addition, ABM can require vast amounts of detailed information with respect to forest agents, such as trees, soils, or hydrology. These agents may have unique parameters. For example, a tree can have diameter, height, health, and vigor. Soils can contain

chemical constituents, texture, and depth. Hydrology may be composed of water quality, volume, and temperature. The collection of the forest agent parameters can be expensive and time consuming. Moreover, modeling a forest landscape using ABM with detailed information requires complex, agent-based interactions that may necessitate a great deal of time to compute, as well as extensive computing power (Perez and Dragicevic 2012). Therefore, ABM is typically applied to extremely small areas (e.g. 1 hectare) (Bauer et al. 2009, Perez and Dragicevic 2012).

Perez and Dragicevic (2012) modeled a forest disturbance due to an infestation of mountain pine beetle (MPB) (*Dendroctonus pondersae* Hopkins.) in the native forests of Canada using a hybrid model. This hybrid MPB model uses ABM, CA, and GIS. The ABM components (i.e. the agents) were the insects interacting with the forest environment (e.g. tree species, tree height, tree diameter), which produced a surface of dead trees. There were three CA components: 1) elevation, 2) aspect, and 3) a surface of dead trees derived from the ABM component coupled with a series of CA rules in a GIS. The model was simulated over time and the output was a surface depicting tree health at some future time period. Due to ABM complexity and computer limitations, the model could not be simulated at the landscape level.

CA modeling structure, rules, and interactions with cells, rather than interactions at the agent level, offer advantages that make CA the preferred choice for modeling the spread of *P. thomsoni* over the landscape when compared to the ABM counterpart. Therefore, CA is the modeling method employed for this study. The objective of this study is to: 1) develop a CA model that simulates the spatial and temporal dynamics of *P. thomsoni* observed from 2006 to 2010 in the Anchorage bowl, 2) conduct a sensitivity analysis on the model, and 3) adapt the model to predict historical and future trends in severity of *P. thomsoni.*

MATERIALS AND METHODS

Study Area

The entire city of Anchorage, Alaska as defined by the United States Census Bureau is 450,850 ha (Figure 1) (ESRI 2007). However, the study area called the Anchorage Bowl is 20,807 ha in size and a subset of the 450,850 ha. The Anchorage Bowl is the location where most residents in Anchorage reside and is the bounding region of the study area. Birch trees (host) are present at some level throughout study area.

In 2006, the US Forest Service (USFS) identified sites for a long-term monitoring network to study the distribution, spread, and severity of *P. thomsoni* in the Anchorage Bowl. The three primary objectives of the study were: 1) examine the trends in severity of *P. thomsoni* in the Anchorage Bowl using various methods to characterize the global averages, 2) generalize the spatial models of the distribution of *P. thomsoni* , and 3) compare and contrast spatial distributions across years (Lundquist et al. 2012) .

Six years of field data (2006 – 2011, inclusively) were collected in the study area; however, only five years of field data were used for model development (2006 – 2010). These data include the intensity (number of lesions on tree leaves) from the *P. thomsoni* larva in the study area. Tree selection was somewhat subjective and limited to public property (i.e. parks, road rights of way, and open spaces). The same trees were resampled from year-to-year whenever possible and the samples were spread throughout the study area. On each tree, technicians selected and pruned a branch from the outer canopy. Fifty leaves were randomly selected from the pruned branch, and the number of leaves with at least one lesion was counted. The results from this technique produced severity values ranging from 0 – 50, where 50 is 100% infested (Lundquist et al. 2012) .

The Model

A CA model was developed to describe the spatial-temporal dynamics of the severity of *P. thomonsi* in the study area, using the statistical programming language R (R Development Core Team 2008) coupled with a library called RandomFields (Schlather 2012). Assume that S_0 represents the severity of the infestation in some region *D* in time period t = 0. The severity in the next time period (S_1) was modeled using the following relationship:

$$S_t = S_{t-1} + \Delta S_t$$

$$\Delta S_t = f\left(S_{t-1}, I_t, t, \varepsilon_t\right) \qquad [2]$$

where ΔS_t is the change in severity observed in time period *t*, which is a function of S_{t-1} the severity of the infestation in the previous time period, I_t an indicator variable identifying if the area of interest is associated with an increase or decrease in severity and ε represents an error term. A flow chart of the model is provided in Figure 2.

Areas of Random Size and Shape

Following is a brief description of the algorithm used to generate areas of random size and shape. The function GaussRF in the R library RandomFields was used to generate a spatially correlated surface with mean zero and variance = 1 (Figure 3A). A Matern covariance function (nugget = 0, range = 1134 m (3685 ft), smoothness = 6) was used to define the spatial structure of the simulated surface. Using these parameters, the function GaussRF generated three-dimensional surfaces with z-values ranging over the interval [-3, 3]. Next, all negative z-values were set to zero (Figure 3B). Finally, the size and shape of the random area was defined as those areas of the truncated surface in which the z-value exceeds some threshold value (Zcut) selected at random. The equation: Zcut = 1.49 - 2.78*R, where R is a random number selected uniformly over the interval [0.1, 0.5] was used to define a threshold such that the

resulting area (Parea) was proportional to the random number (Figure 4). The Zcut equation was empirically derived from a series of model simulations. In the example depicted in Figure 3C, the random number 0.43 (Zcut = 0.30) generated an area that covered 27% of the study area (Figure 3C), while the random number 0.14 (Zcut = 1.10) generated an area that covered 4% of the study area. The algorithm generates areas that cover anywhere from 3% to 69% of the study area, with an average of 26.7% (Figure 5).

Calibration

To evaluate the algorithm for generating areas of random size and shape, the areas of overlap between successive areas generated at random were examined. Let *A* and *B* represent two areas generated at random with areas $\mathcal{A}(A)$ and $\mathcal{A}(B)$, respectively. It is also assumed that the process is restricted to a particular region *D* with area $\mathcal{A}(D)$. Then, *A* and *B* are independently and identically distributed (iid) uniformly on *D*, i.e.

$$\mathrm{P}(A \in D, B \in D) = \mathrm{P}(A \in D)\,\mathrm{P}(B \in D) = \frac{\mathcal{A}(A)}{\mathcal{A}(D)}\frac{\mathcal{A}(B)}{\mathcal{A}(D)} \qquad [3]$$

Uniformity refers to the fact that events in question exhibit no tendency to occupy particular regions of the study area, while independence suggests that the location of a given event is determined without reference to any other event. Under these conditions, the conditional probability of observing *A* given *B* (i.e. area *B* overlaps area *A*) is given by:

$$P(A \mid B) = \frac{P(A \in D, B \in D)}{P(B \in D)} = P(A) = \frac{\mathcal{A}(A)}{\mathcal{A}(D)} \qquad [4]$$

This suggests that the proportion of overlap of areas generated at random should equal the area of the random shapes expressed as a proportion of the total area.

Empirical evidence provided five estimates of the overlap of regions experiencing an increase in severity. Depending on the number of years separating these random events, the

amount of overlap varies. If there is at least two years separating the random events, the amount of overlapping area observed was 19%, 22% and 24%. The algorithm generates areas of random size and shape with an overlap ranging from 0% to 65%, with an average overlap of 26.9% (Figure 6). The areas of overlap generated by the algorithm are in close agreement with the empirical data, indicating that the areas generated by the algorithm to identify areas in which the severity of *P. thomsoni* increases are of the appropriate size. The similarity of the distribution of the area of overlap with the distribution of the relative size of the random areas (Figure 6) is supported by the relationship expressed in Equation 4.

If the random events were sequential in time, the observed overlap for three years was 10%, 10% and 11%. To account for this difference, Zcut was multiplied by 1.85. This generated areas of random size and shape that are sequential in time and with an overlap ranging from 3% to 62%, with an average of 12.2% (Figure 7).

Trend Surface Model

Regression analysis was used to describe the change in severity of individual sample trees in each time period using the model:

$$\Delta S_t = \beta_0 + \beta_1 S_{t-1} + \beta_2 I_t + \varepsilon_t \qquad [5]$$

where I_t is an indicator variable that takes on the value of zero if the severity of the sample tree decreased and one if the severity increased in time period *t*, β_0 and β_2 are the intercepts and β_1 is the slope, and where the other variables are as previously defined.

Regression analysis was used to test the null hypothesis that the regression coefficients in Equation 5 are independent of time. If the null hypothesis was rejected, regression models were developed to describe how the regression coefficient changed with time. Regression models with different functional forms (i.e., linear, quadrate, log, cosine, etc.) were evaluated.

The error component of the trend surface model (Equations 2 and 5) was simulated using the function GaussRF to generate a spatially correlated surface, with mean zero and variance of 4. A Matern covariance function (nugget = 0, range = 1134 m (3685 ft), smoothness = 3) was used to define the spatial structure of the simulated surface of the errors. The error surface was added to the trend surface model to represent the variability in severity across the bounded region *D* in a given time period.

Model Evaluation

Monte Carlo simulations were used to evaluate the model in estimating the change in severity during 2006-2011. The model requires a surface representing the severity in the base, or starting year (2006). The function GaussRF used in generating the random groups was used to generate a spatially correlated surface, with a mean severity of 26.9 and variance of 3. A Matern covariance function (nugget = 0, range = 1134 m (3685 ft), smoothness = 3) was used to define the spatial structure of the simulated surface of the severity in 2006. The model was simulated 100 times per time period and information on the minimum, maximum, and average severity in each time period was recorded. The information on the minimum and maximum values were used to construct a 99% simulation envelop around estimates of the average severity. If the observed severity values were contained within the simulation envelops, there was not enough evidence to reject the null hypothesis that the model adequately described the changes in severity of *P. thomsoni* over the time period of interest.

Sensitivity Analysis

Sensitivity analysis was performed to evaluate the impact of changing key input parameters about which there is some uncertainty on estimates of the average severity of the *P. thomsoni* infestation over the time period 2006-2018. The results of the sensitivity analysis were presented in the form of graphs.

Base model (2006): $\mu = 26.9$, $\sigma^2 = 3$, CV = $\sigma/\mu = 0.064$.

1. Increase the mean severity in the base year: $\mu = 40$; $\sigma^2 = 3$, CV = 0.043.

2. Decrease the mean severity in the base year: $\mu = 10$; $\sigma^2 = 3$, CV = 0.173.

3. Increase the mean severity and variance in the base year: $\mu = 40$; $\sigma^2 = 6.6$, CV = 0.064.

4. Decrease the mean severity and variance in the base year: $\mu = 10$; $\sigma^2 = 0.41$, CV = 0.064.

Error surface associated with the trend surface model: $\mu = 0$; $\sigma^2 = 4$.

5. Increase variability in the error surface: $\sigma^2 = 8$.

6. Decrease variability in the error surface: $\sigma^2 = 2$.

Change the parameters of the regression model used to predict the intercept of the trend surface model describing the change in severity of trees in an area of decreasing severity.
$\hat{\beta}_{ot} = \alpha_0 + \alpha_1 f(t) + \varepsilon_t$.

7. Decrease the value of the intercept: -6.0

8. Decrease the value of the intercept: -8.0

9. Reduce the slope: 0.7

Change the parameters of the regression model used to predict the intercept of the trend surface model describing the change in severity of trees in an area of increasing severity.
$\hat{\beta}_{02t} = \alpha_0 + \alpha_1 f(t) + \varepsilon_t$.

10. Decrease the value of the intercept: 12

11. Increase the value of the intercept: 25

Change the parameters of the regression model used to predict the slope of the trend surface model. $\hat{\beta}_{1t} = \alpha_0 + \alpha_1 f(t) + \varepsilon_t$.

12. Increase the value of the intercept: -0.1

13. Decrease the value of the intercept: -0.4

Results of the sensitivity analysis were used to identify key parameters that could be modified to simulate the start of the infestation as close to the first sighting of *P. thomsoni* and to match with the observed data in 2006. A Chi-squared type of goodness-of-fit statistics was used to evaluate the fit of the different scenarios evaluated.

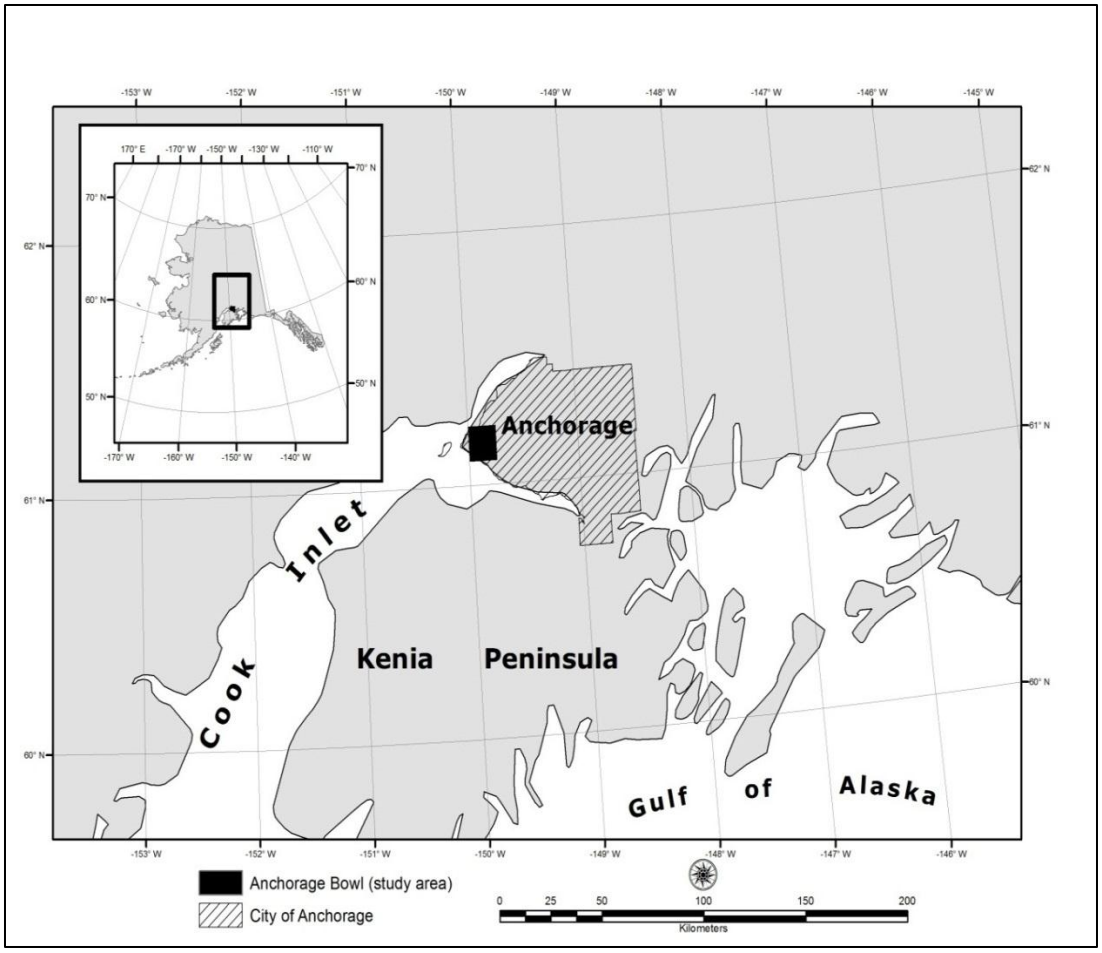

Figure 1. Study area for modeling the spatial and temporal change in severity of *P. thomsoni* in the Anchorage Bowl, Alaska.

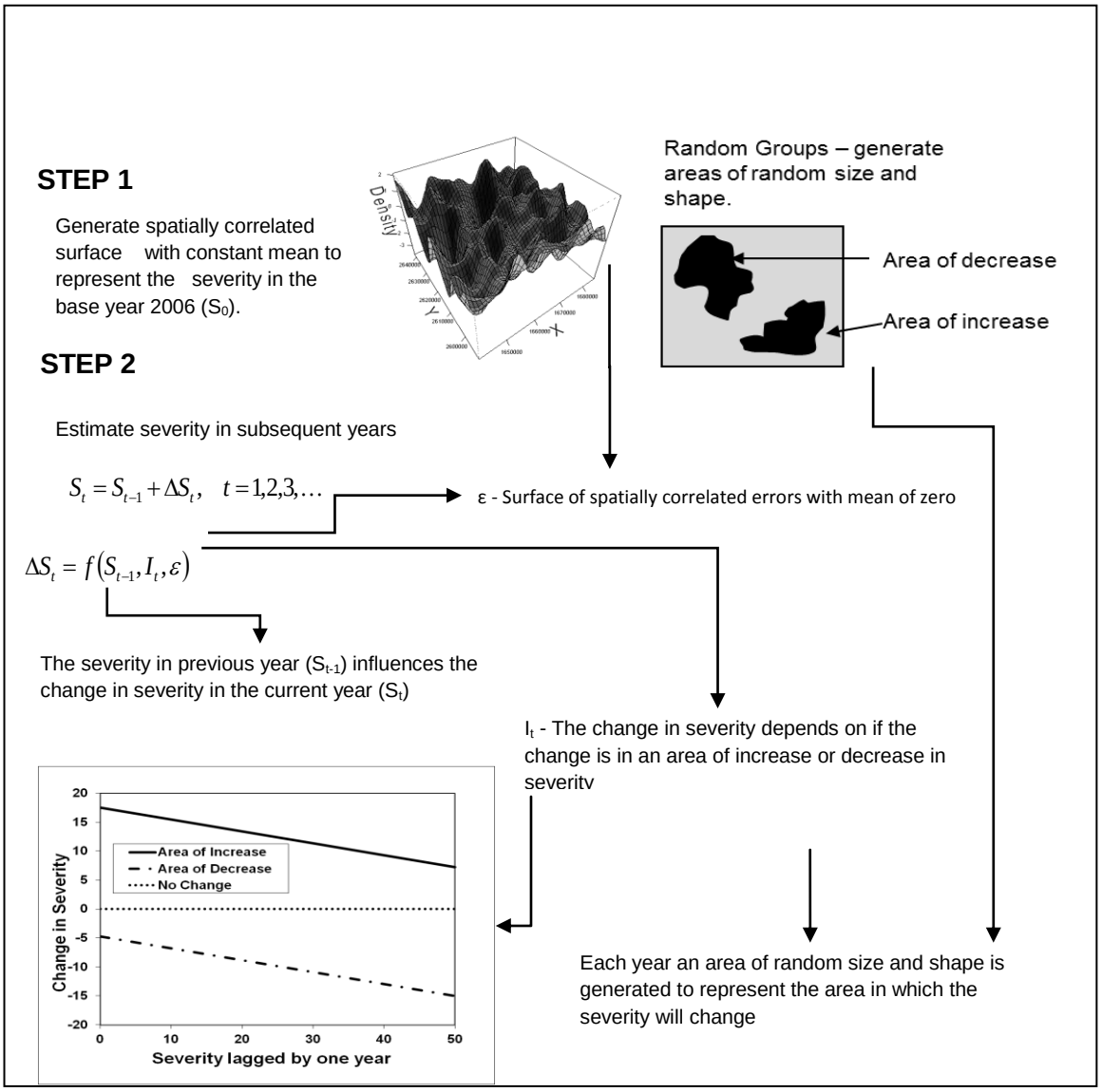

Figure 2. A model flow chart illustrating the various steps and processes used for modeling the severity of *P. thomsoni* in the Anchorage Bowl, Alaska. The model consists of two main components. The first component is an algorithm that generates areas of random size and shape (e.g. random groups) within some bounded region *D* to represent areas in which the severity will increase. The second component of the model is a trend surface model that describes how the severity changes over time depending on if the change in severity is associated with an area in which the severity increases or decreases.

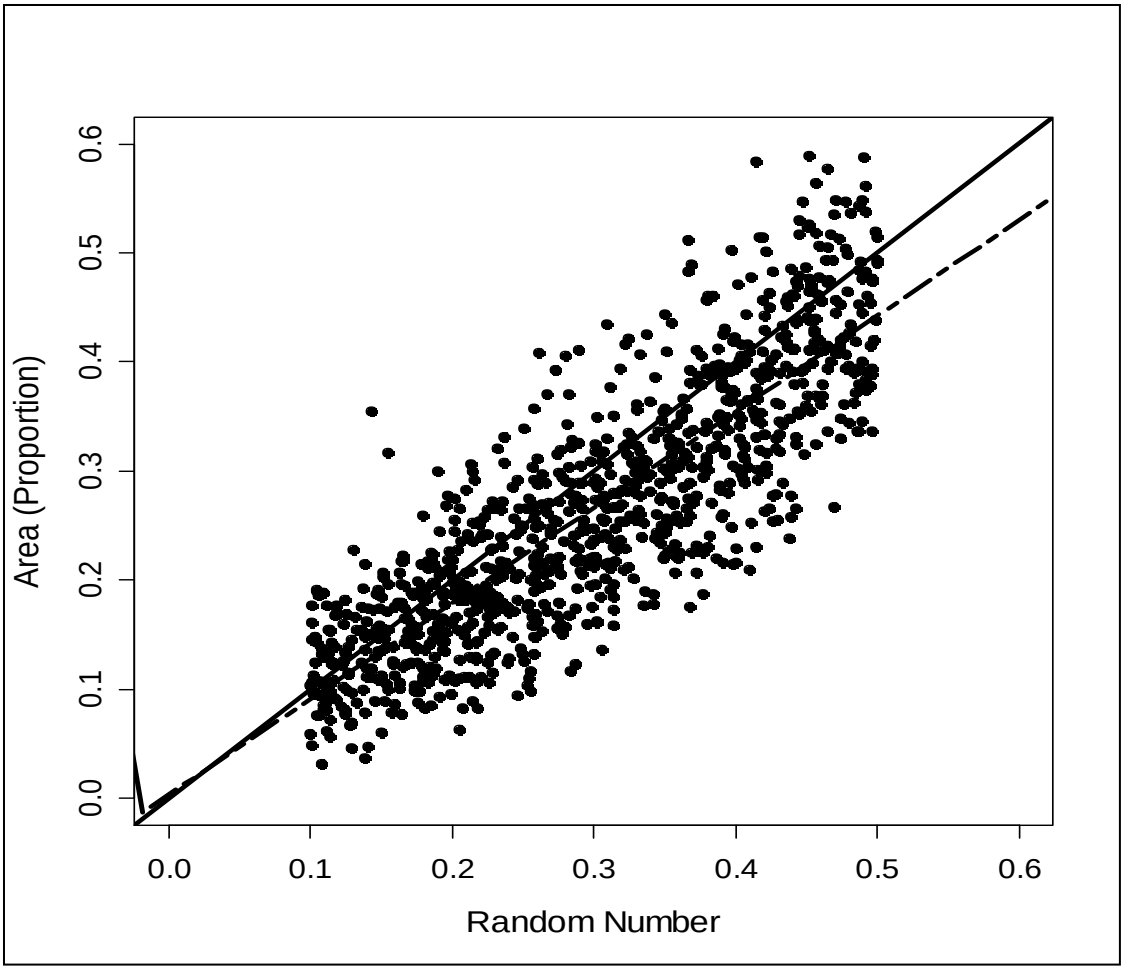

Figure 3. Scatter plot depicting the relationship between the random number (R) and the area of the random shapes expressed relative to the total study area (Parea). The solid line has a slope of one, while the dashed line is the line of best fit. The data is from 1,000 simulations of the algorithm used to generate areas of random size and shape for the *P. thomsoni* spread model in the Anchorage Bowl, Alaska.

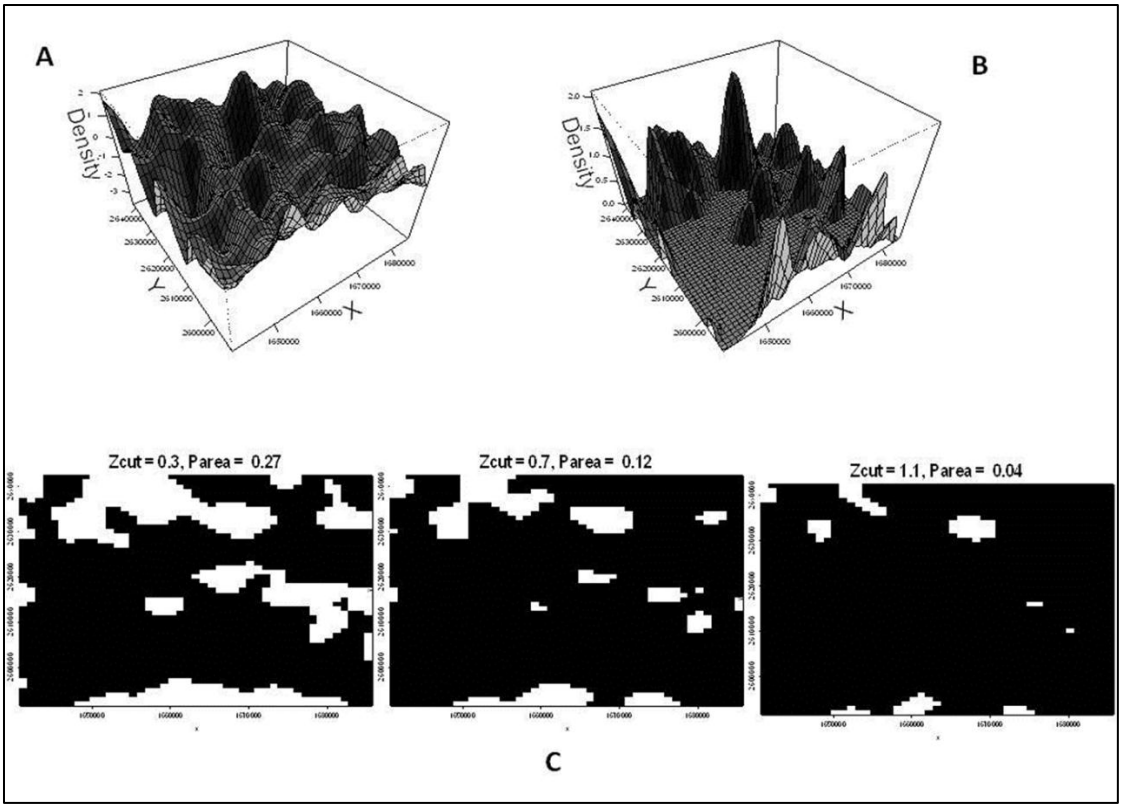

Figure 4. Steps used to generate areas of random size and shape to identify areas in which the severity of *P. thomsoni* increases or decreases in the Anchorage Bowl, Alaska. A) Step 1 – Generate a spatially correlated random field (parameters: $\mu = 0$, $\sigma^2 = 1$, θ (smoothness) = 6, range = 3685 ft, nugget = 0, model = Matern); B) Step 2 – truncate negative values (Z-scale) to zero; c) Step 3 – generate a random number uniformly over the interval 0.1 to 0.5 (Zcut) to create a binary surface from B. Values greater than Zcut represents the area of random size and shape associated with an increase in severity (1 = white), while values less than Zcut represent areas associated with a decrease in severity (0 = black). The variable Parea is the proportion of the total area associated with the area delineated as an increase in severity.

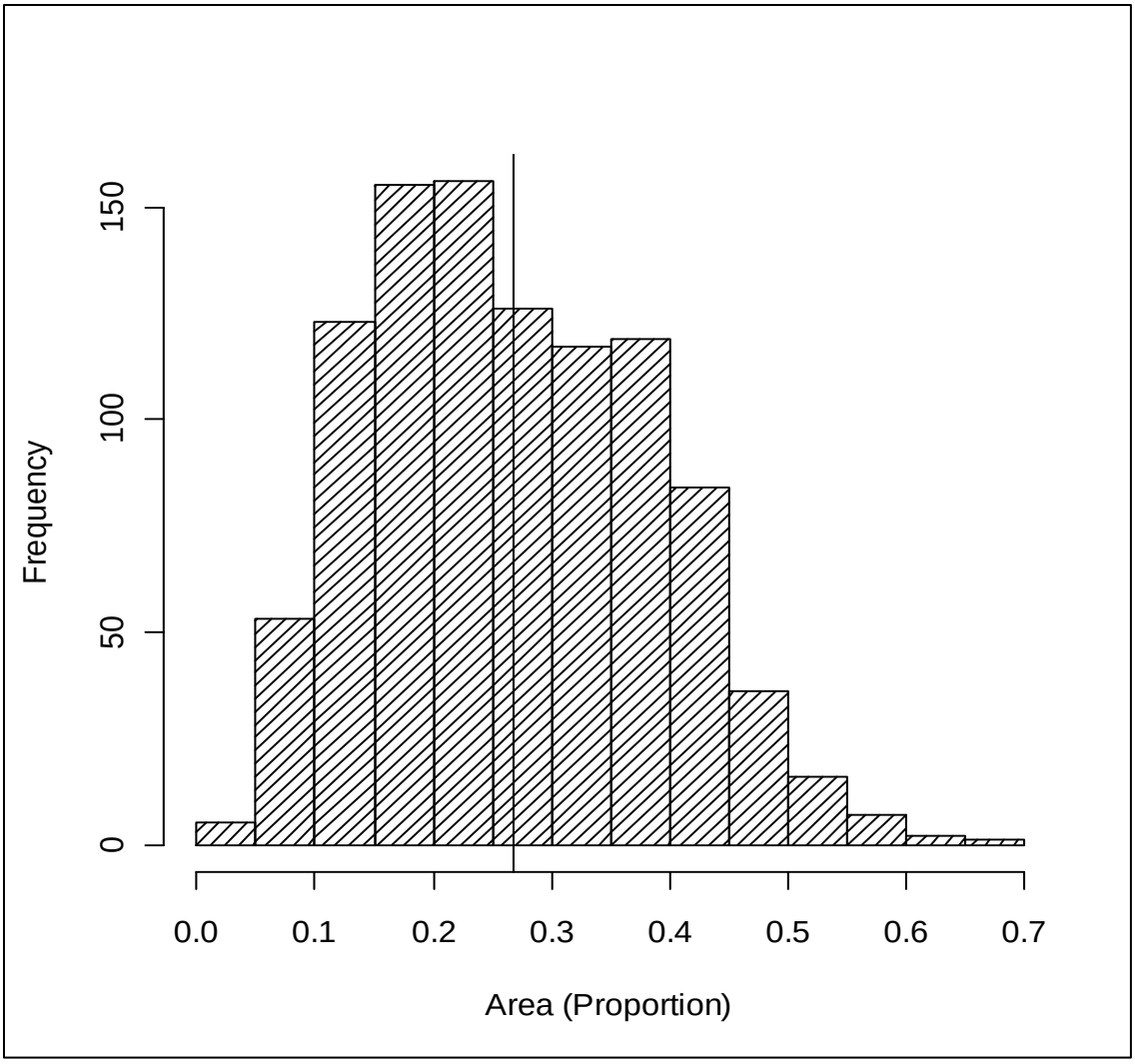

Figure 5. Histogram of 1000 areas, expressed as a proportion of the total area (Parea) in the Anchorage Bowl, Alaska, study area for *P. thomsoni* infestation. This histogram was created using the algorithm to generate areas of random size and shape. The algorithm generated areas that covered anywhere from 3% to 69% of the study area, with an average of 26.7% (solid vertical line).

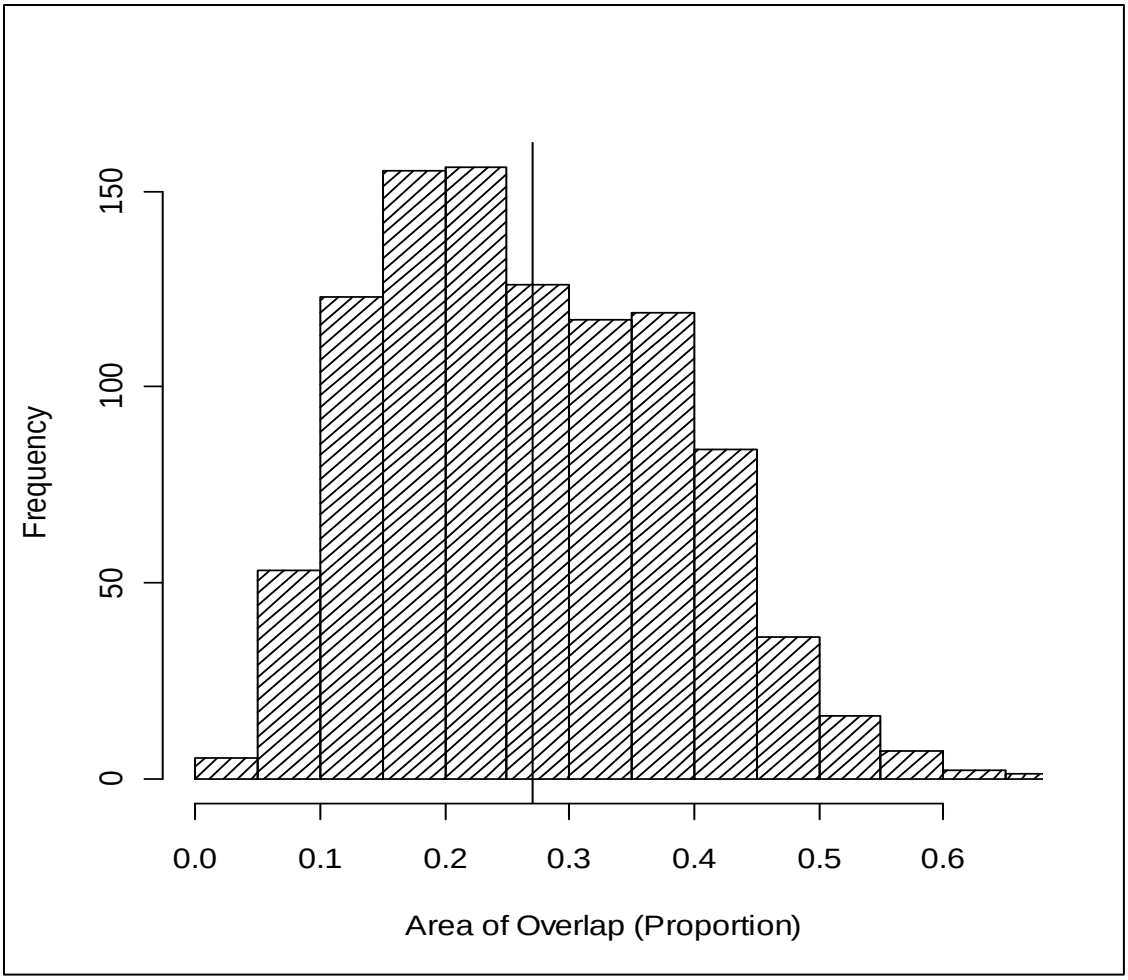

Figure 6. Histogram of 1,000 areas of overlap, expressed as a proportion, of two independent areas created using the algorithm to generate areas of random size and shape in the Anchorage Bowl, Alaska, study area for *P. thomsoni* infestation. The algorithm generated areas of overlap that covered anywhere from 0% to 65% of the second random area, with an average of 26.9% (solid vertical line).

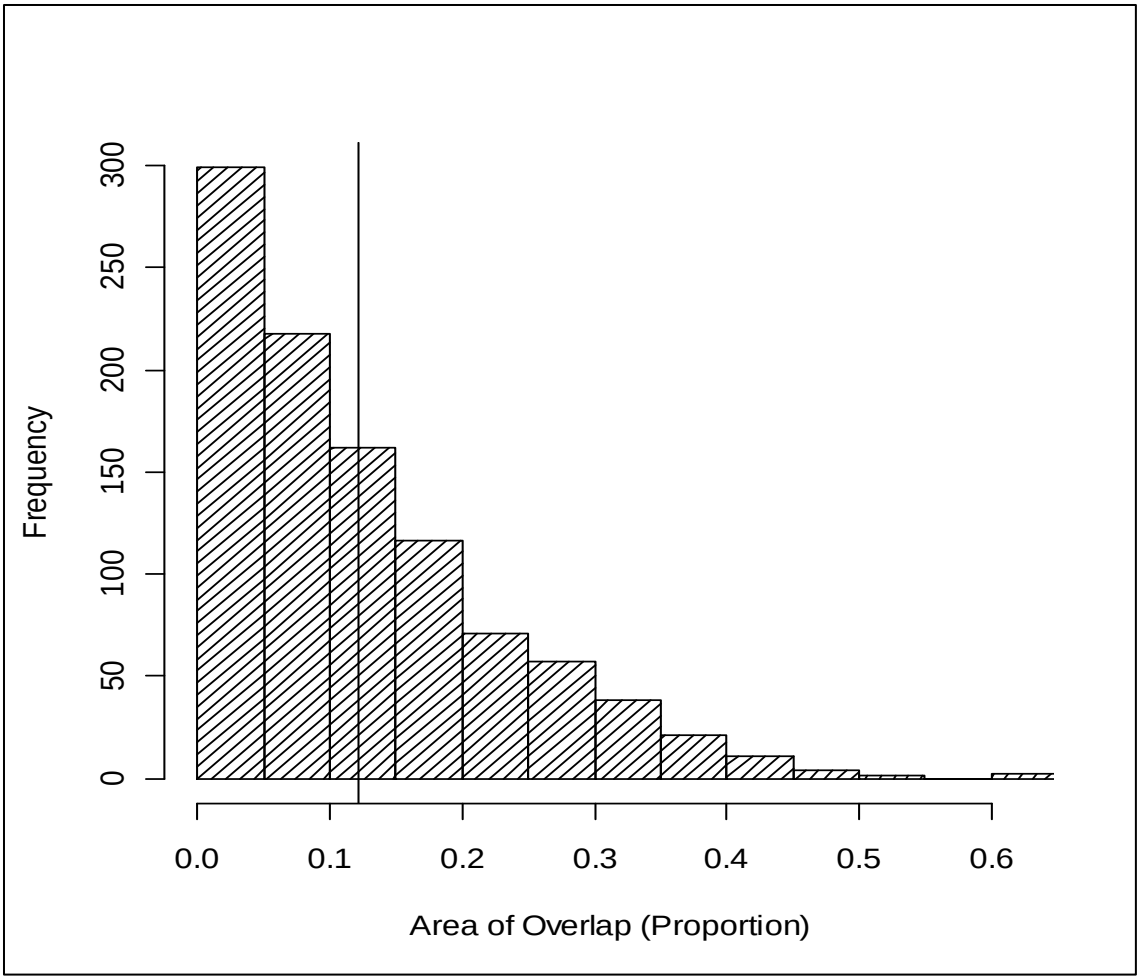

Figure 7. Histogram of 1,000 areas of overlap, expressed as a proportion of two independent areas created using the algorithm to generate areas of random size and shape in the Anchorage Bowl, Alaska, study area for *P. thomsoni* infestation. The algorithm generated areas of overlap that are sequential in time and covered anywhere from 3% to 62% of the second random area, with an average of 12.2% (solid vertical line).

RESULTS

Trend Surface Model

The fitted regression models used to describe the change in severity of *P. thomsoni* in each of the four time periods are summarized in Table 1. The regression models had R^2 values ranging from 0.58 (T2) to 0.66 (T3). A plot of the fitted model for the 2006 – 2007 time period (T1) is displayed in Figure 8 and depicts how the average severity changed in areas that showed an increase in severity (solid line) and in areas that showed a decrease in severity (dashed line) as a function of the severity in the previous time period. In areas experiencing an increase in the severity of the infestation, heavily infested trees were unable to increase in severity as much as the lightly infested trees. This could be thought of as a density-dependent factor influencing the ability of the infestation to exceed some upper limit on the severity of the infestation. In contrast, heavily infested trees were able to substantially reduce the severity of their infestation compared to lightly infested trees. This could be thought of as a plant defense mechanism.

The next step in the analysis was to develop models to describe how the regression coefficients in Table 1 change over time. Various regression models were evaluated to select a functional form (i.e. linear, quadratic, log, and cosine) that best fit the data and had good asymptotic and harmonic properties when the model was used to simulate the infestation into the future. The two intercepts terms, $\hat{\beta}_0$ and $\hat{\beta}_{02}$ were modeled using a natural log function while the slope, $\hat{\beta}_1$ was modeled using a cosine function (Table 2). It was observed that a stronger temporal correlation existed between $\hat{\beta}_{02}$ than with the coefficient $\hat{\beta}_2$. As a result, estimates of $\hat{\beta}_2$ were obtained by subtraction ($\hat{\beta}_2 = \hat{\beta}_{02} - \hat{\beta}_0$). While the log models did not necessarily have the best fit, they asymptotically approached an upper or lower limit unlike other functional forms evaluated. Both log models had R^2 values around 0.90. A cosine model was selected to describe the change in the slope coefficient $\hat{\beta}_1$ over time to mimic the harmonic or cyclic changes

associated with some insect populations (Haynes et al. 2009). A six-year cycle best described the data centered on year three of the study. These harmonic changes can be driven by predation from natural enemies, environmental changes, or density-dependent factors. The fitted models accounted for 76% of the variability observed in the estimated regression coefficients.

Plots of the fitted models are displayed in Figures 9 through 11. Perspective plots of the full model are displayed in Figures 12 and 13, which show how the changes in severity (ΔS_t) varied over time and the influence of the severity in the previous year for the areas associated with a decrease and increase in severity, respectively.

Model Evaluation

The results of running the model 100 times simulate the changes in the severity of the infestation of *P. thomsoni* from 2006 – 2011 is shown in Figure 14. The observed changes in severity fell within the 99% simulation envelop and closely followed the predicted mean severity over this time period, thereby validating the model. In 2011, the predicted mean severity equaled the observed mean severity of nine. This latter estimate of severity was not used in developing the model; moreover, it provides additional evidence to evaluate the overall fit of the model.

To further evaluate the model, comparisons were conducted to determine how the severity changed over time in areas exhibiting an increase (Figure 15) or a decrease (Figure 16) in severity. The simulated trend closely resembled the observed trend over time. The simulated model tended to overestimate the increase in severity in all the time periods. An important consideration was that the model mimicked the observed trends in the data and not necessarily the absolute differences between the estimates of the severity from the simulation model and the field data.

Sensitivity Analysis

The sensitivity analysis was conducted on selected model parameters. All sensitivity analysis was done for a 12-year period (2006 – 2018) and 100 iterations. Results were summarized for each analysis in the form of a graph.

Changes in the base model

Changes in base model were implemented by changing the mean (μ) and variance (σ^2) (Figure 17). This addresses how sensitive the model was to changes in these two variables of the base input model. Through inspection, it was observed that changing μ from the base values of 26.9 to 10 or 40 made a significant change in the level of severity in the first three years (t = 1 to t = 3) of the simulations (Figure 17 lines B, C, D, and E). This was intuitive and expected. Beginning a simulation with a different mean value will indeed produce results reflecting the differences in the mean over time. Changing σ^2 from a base value of 3 to either 6.6 or 0.41 (lines C and E Figure 17, respectively) had little effect on the predicted mean severity; however, changing the variance influenced the width of the simulation envelop. As the variability in the severity in the base year increased, the width of the simulation envelop also increased. An interesting observation of Figure 17 illustrates that after four years, regardless of μ or σ^2, the predicted mean severity begins to converge (line A Figure 17) and, after ten years, the estimates of the mean severity are nearly identical.

Changes in the error surface model

Changing the variability in the random error surface had little influence on the estimates of the mean severity over time (Figure 18). It did, however, influence the width of the simulation envelop: the more variability in the error surface, the wider the simulation envelops.

Changes in the ability of a tree to recover

Changes in the intercept and slope of the log model used to describe the change in the intercept term $\hat{\beta}_0$ in the trend surface model are displayed in Figure 19. Increasing the rate (i.e.

$\hat{\beta}_0$ becoming more negative) at which a lightly infested tree recovers from an infestation reduces the predicted mean severity over the period of the simulation (Figure 20). Reducing the rate at which the intercept decrease over time also led to a decreased in the predicted mean severity. A tree can retain its ability to recover from an infestation, thereby lowering the overall level of severity.

Changes in the ability of a tree to become infested

Changes in the intercept ($\hat{\beta}_{02}$) of the log model are provided in Figure2. The $\hat{\beta}_{02}$ intercept represents the susceptibility of the tree to become infested. Increasing the sensitivity of a tree to infestation increases the predicted mean severity, while a decrease in sensitivity decreased the predicted mean severity (Figure 22). Sensitivity as used here refers to a tree's ability to defend itself against an infestation.

Changes in the slope of the trend surface model

Changes in the intercept of the cosine model describing how the slope ($\hat{\beta}_1$) of the trend surface model changed over time are depicted in Figure 23. As the rate of decrease increased, the predicted mean severity decreased (Figure 24). As the slope of the trend surface model became more negative, density-dependent factors limited the ability of *P. thomsoni* to increase the severity of the infestation and increased a tree's ability to recover from an infestation. The net result was an overall decrease in the level of severity.

Hindcasting and Forecast the Severity of the *P. thomsoni* Infestation

The model was modified to simulate the initial phase of the simulation and to identify the year the infestation started (i.e. hindcasting). The sensitivity analysis identified the parameters of the trend surface model associated with a trees susceptibility to become infested $\hat{\beta}_{02}$ as the most responsive to simulate the rapid increase in the initial phase of the infestation. Three simulations were run for a 20-year time period (1998 – 2018) during which the parameter $\hat{\beta}_{02}$ was multiplied

by an expansion factor of 2.5, 2.75, and 3. A plot of the predicted mean severity over the 20-year time period was evaluated for correspondence to the observed severity levels (2006 – 2010). A Chi-square type goodness-of-fit was calculated to select the best fitting scenarios. Results of this analysis are summarized in Table 3 and the final model is presented in Figure 25.

The results from the simulation from the time period 1998 to 2018 indicated that the expansion factor of 2.75 provided the best model. The expansion factor allowed the change in mean severity of *P. thomsoni* to increase from 1998 until at least 83% of the study area was infested. At this point, the model parameters were allowed to proceed as usual and the expansion factor was removed.

The results of the modeling indicate the infestation began in 1998, at which time it was assumed the average severity was near zero. The severity of the infestation increased rapidly, reaching a peak in 2004 with an average severity of 37.2. During this time period, the trees were assumed to have no defenses against *P. thomsoni*. Density-dependent factors were in play by limiting the rate in which heavily infested trees could increase in severity. It took on average six years for the infestation to spread throughout the Anchorage Bowl. After six years, there was very little area available for new infestations. As a result, *P. thomsoni* must begin to reinfest areas. At this point, plant defenses began to limit the ability of *P. thomsoni* to heavily infest a tree. Increased population sizes of local parasitoids may also play a role in the decreased trend in severity. The severity continued to decrease until the 2010 – 2011 time period, at which time the severity leveled off.

Table 1. Regression models coefficients predicting the change in the severity (ΔS_t) of *P. thomsoni* in the time period *t* as a function of the severity of the infestation in the previous time period (S_{t-1}) and if the trees are located in an area associated with an increase ($I_t = 1$) or decrease ($I_t = 0$) in severity in time period *t*. The numbers in parentheses are the estimated standard errors.

Coefficient	Time Period			
	T1	T2	T3	T4
β_0	-4.723 (1.967)	-3.208 (1.725)	-2.619 (1.411)	-2.735 (1.043)
β_1	-0.206 (0.056)	-0.342 (0.054)	-0.418 (0.055)	-0.291 (0.046)
β_2	22.244 (1.802)	16.891 (1.946)	17.387 (1.653)	15.646 (1.173)
R^2	0.630	0.580	0.657	0.635
s_{xy}	9.020	9.020	8.962	7.068
n	132	132	150	150

Table 2. Regression models predicting how the regression coefficients of the model describing the change in the severity $\Delta S_t = \hat{\beta}_0 + \hat{\beta}_1 S_{t-1} + \hat{\beta}_2 I_t$ of *P. thomsoni* in a given time period (t = 1, 2, 3,…) changes with time. The numbers in parentheses are the estimated standard errors. Note $\hat{\beta}_2 = \hat{\beta}_{02} - \hat{\beta}_0$.

Variable	$\hat{\beta}_0$	$\hat{\beta}_1$	$\hat{\beta}_{02}$
Intercept	-4.538 (0.332)	-0.255 (0.022)	17.055 (1.098)
ln(*t*)	1.532 (0.349)		-2.930 (1.156)
cos(*t*-3)		-0.142 (0.033)	
R^2	0.910	0.900	0.760
s_{xy}	0.364	0.034	1.203
n	4	4	4

Table 3. Expansion factor – The factor used to increase the rate of infestation relative to that observed in 2006. Chi-square measure of the goodness-of-fit (GOF) of the observed and expected severity over the time period: 2006-2011. The observed severity in 2006 was equal to 26.9.

Expansion Factor	Start of Infestation	Maximum Severity	Year of Maximum severity	Severity in 2006	Chi-square GOF
2.5	1999	33.3	2005	27.6	1.58
2.75	**1998**	**37.2**	**2004**	**28.5**	**1.11**
3.0	1998	42.7	2004	31.1	1.48

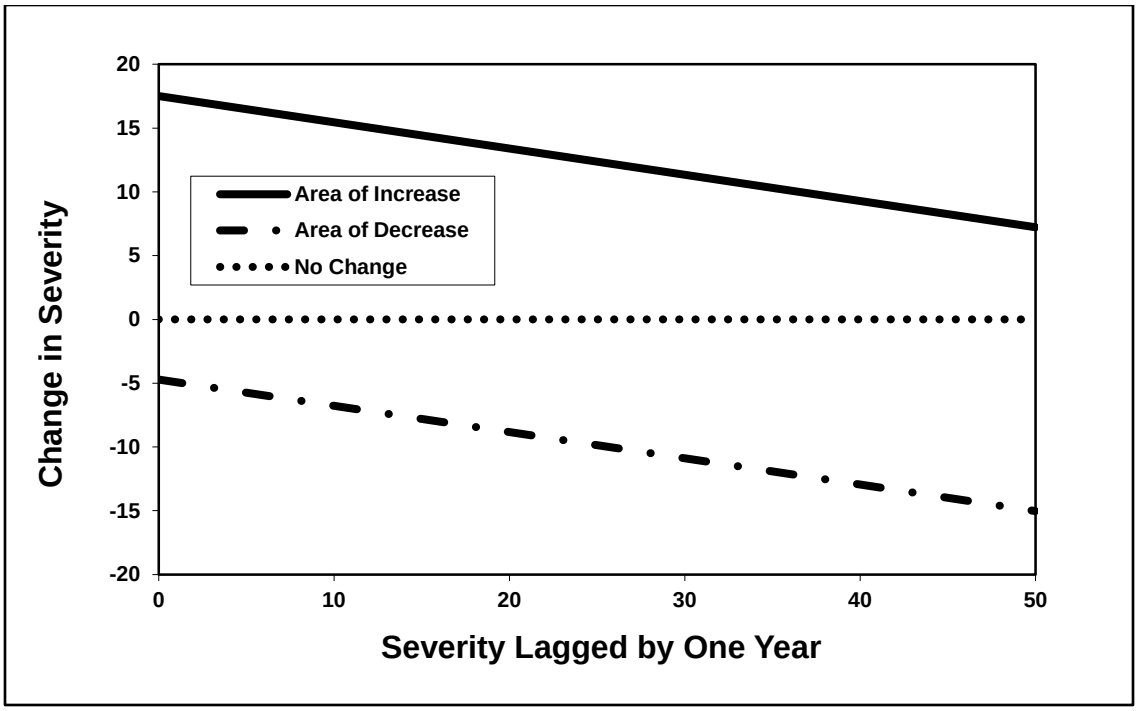

Figure 8. The output results for a single year of the trend surface model. The graph shows changes in the severity of *P. thomsoni* in the Anchorage Bowl, Alaska.

$\Delta S_t = \hat{\beta}_0 + \hat{\beta}_1 S_{t-1} + \hat{\beta}_2 I_t$ where ΔS_t = change in severity for current year, and $\hat{\beta}_0$ = Intercept, $\hat{\beta}_1$ = slope, $\hat{\beta}_2$ = intercept, s_{t-1} = change in severity previous year. The upper graph shows areas with increasing severity (($I_t = 1$) . The lower graph shows areas with decreasing severity ($I_t = 0$) and the middle graph shows areas of no change. $\hat{\beta}_0$, $\hat{\beta}_1$, and $\hat{\beta}_2$ are separate regression equations: $\hat{\beta}_2 = \hat{\beta}_{02} - \hat{\beta}_0$.

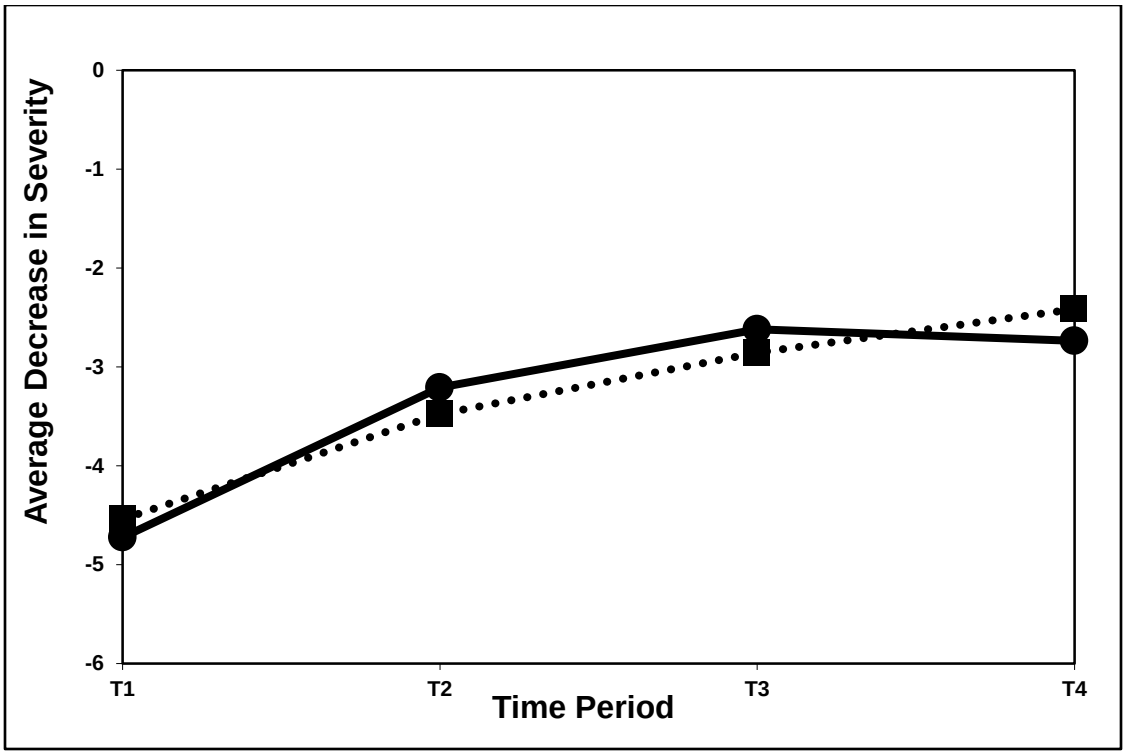

Figure 9. The change over time of the regression coefficient $\hat{\beta}_0$ in the trend surface model describing the changes in severity (ΔS_i) of *P. thomsoni* in the Anchorage Bowl, Alaska, from 2006 - 2010. The solid line represents observed regression line and the dotted line represents the fitted log model, where T1 = change in time from 2006 – 2007.

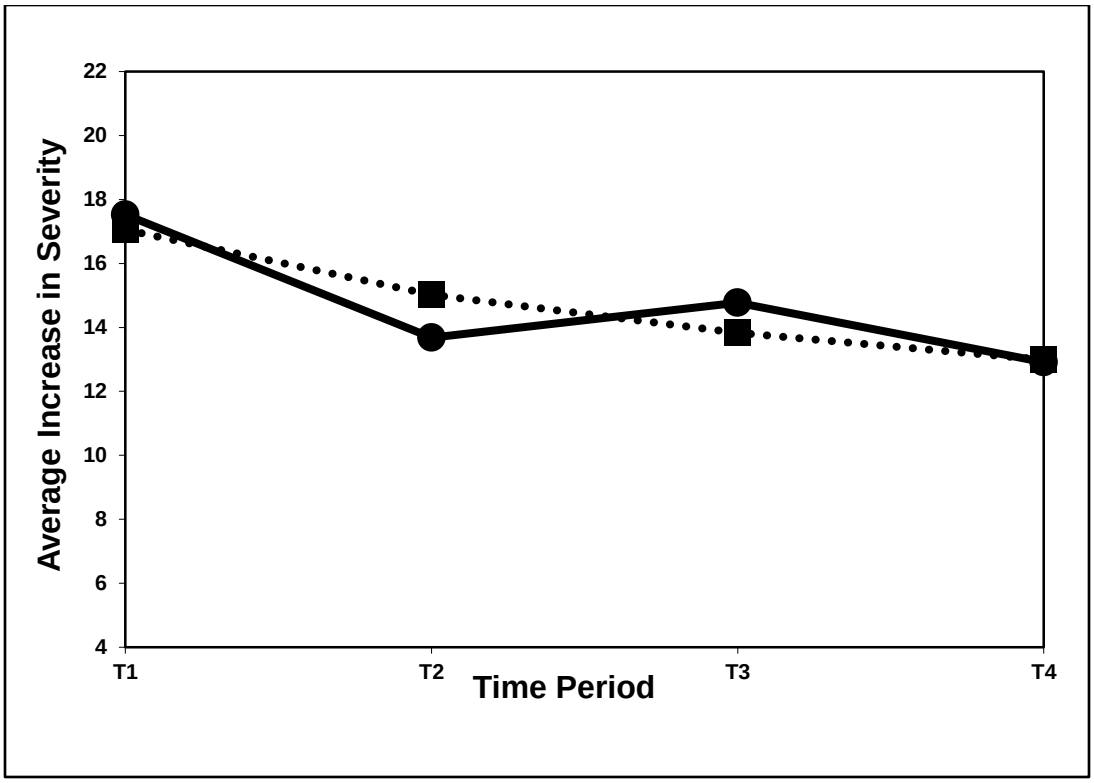

Figure 10. The change over time of the regression coefficient $\hat{\beta}_{02}$ in the trend surface model describing the changes in severity (ΔS_i) of *P. thomsoni* in the Anchorage Bowl, Alaska, from 2006 - 2010. The solid line represents observed regression line and the dotted line represents the fitted log model, where T1 = change in time from 2006 – 2007.

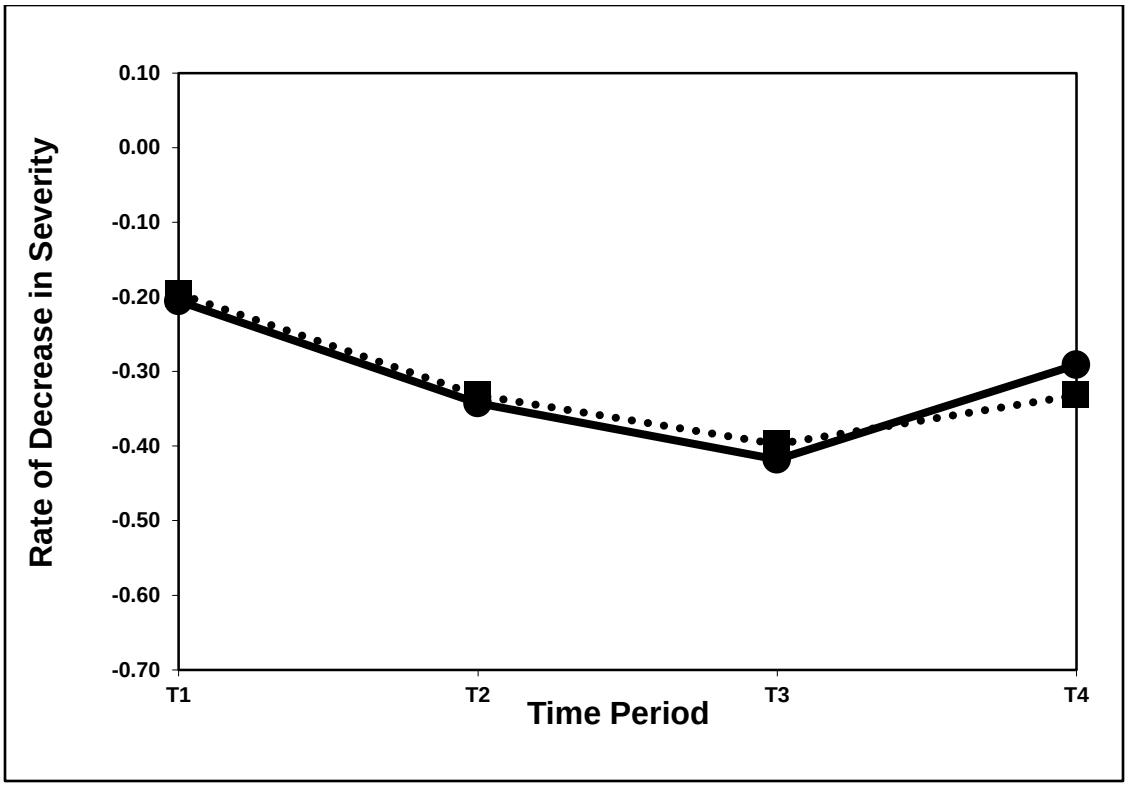

Figure 11. The change over time of the regression coefficient $\hat{\beta}_1$ in the trend surface model describing the changes in severity (ΔS_i) of *P. thomsoni* in the Anchorage Bowl, Alaska, from 2006 - 2010. The solid line represents observed regression line and the dotted line represents the fitted log model, where T1 = change in time from 2006 – 2007.

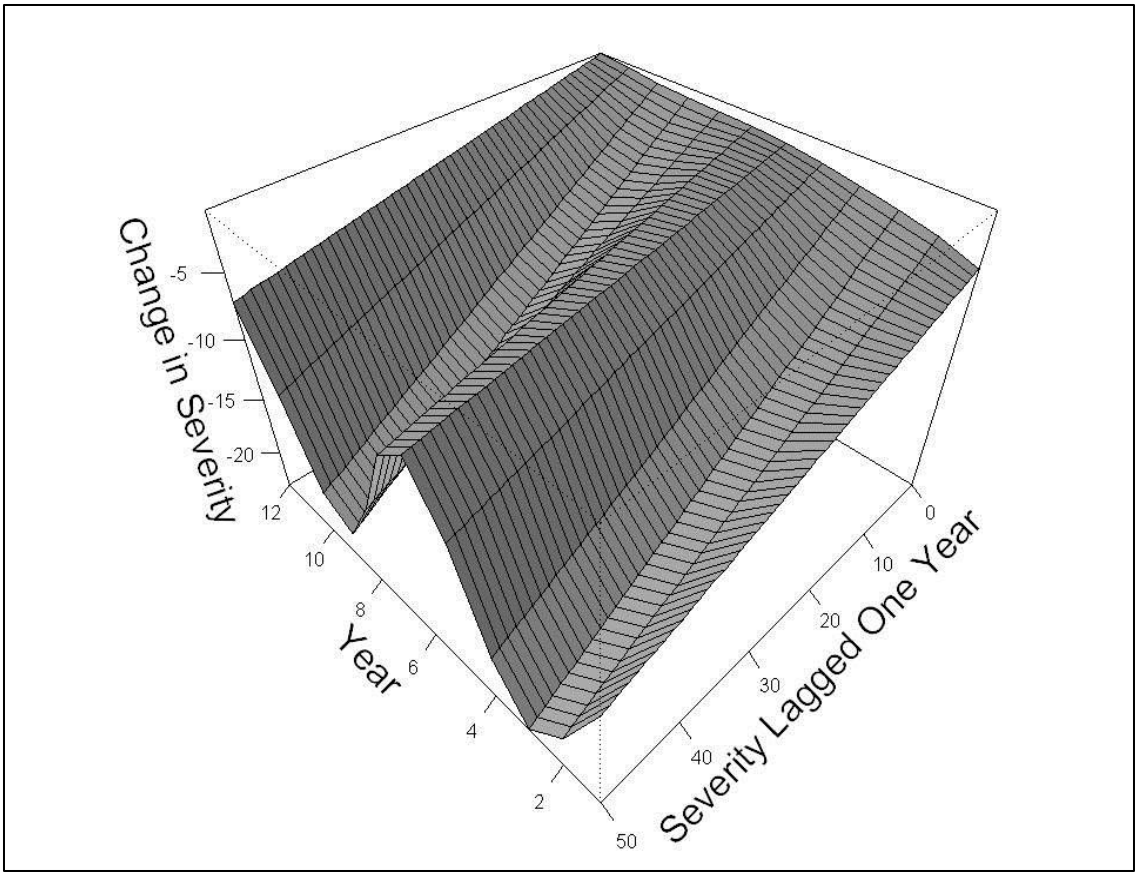

Figure 12. Perspective plot of areas of decrease $I_t = 0$, showing how the change in severity (ΔS_t) is influenced by the year and the severity lagged by one year (s_{t-1}) for the severity of *P. thomsoni* in the Anchorage Bowl, Alaska, when year = 6 = actual year 2006.

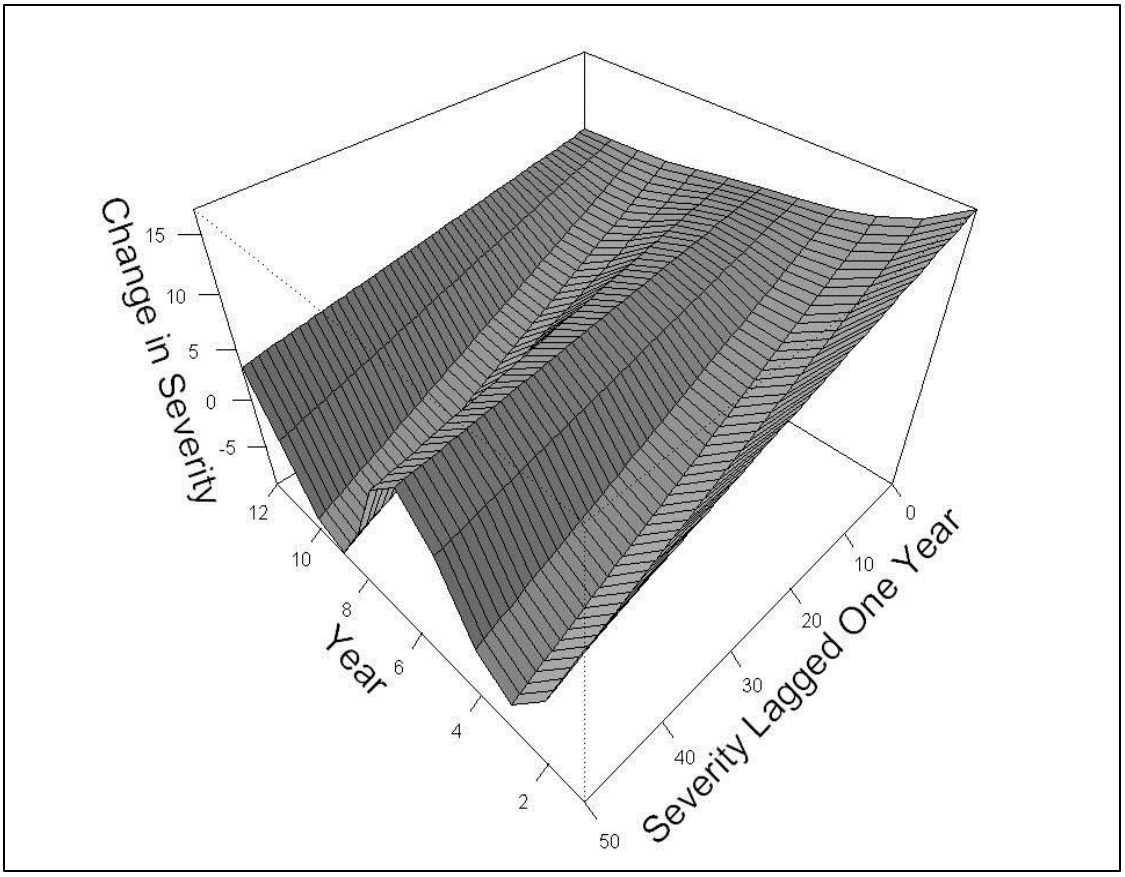

Figure 13. Perspective plot of areas of increase $I_t = 1$, showing how the change in severity (ΔS_t) is influenced by the year and the severity lagged by one year (s_{t-1}) for the severity of *P. thomsoni* in the Anchorage Bowl, Alaska, when year = 6 = actual year 2006.

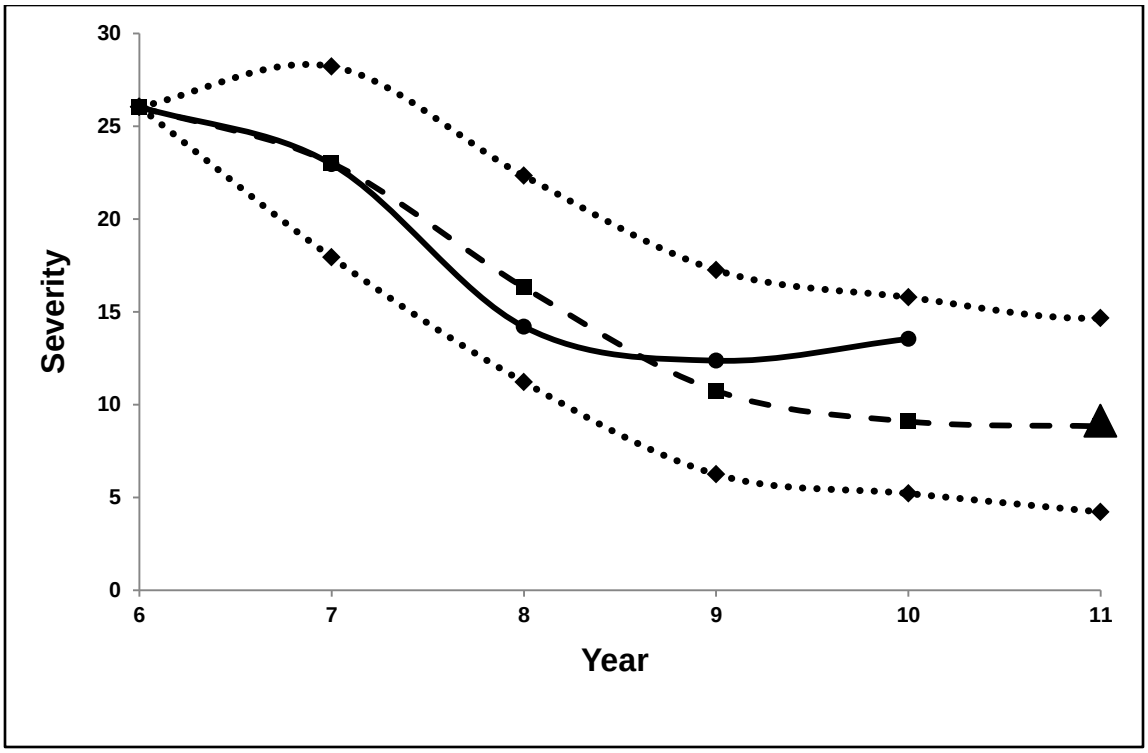

Figure 14. Observed (solid thick line) and predicted (dashed line) changes in the severity of the *P. thomsoni* infestation in the Anchorage Bowl (study area), Alaska, from 2006 to 2011. The dashed line represents the average prediction severity while the dotted lines represent the upper and lower 99% simulation envelop from 100 realized of the simulated model. The triangle symbol at the 2011 time period is the mean observed severity for 2011. This observed data point for the year 2011 was not used for model generation, when year = 6 = actual year 2006.

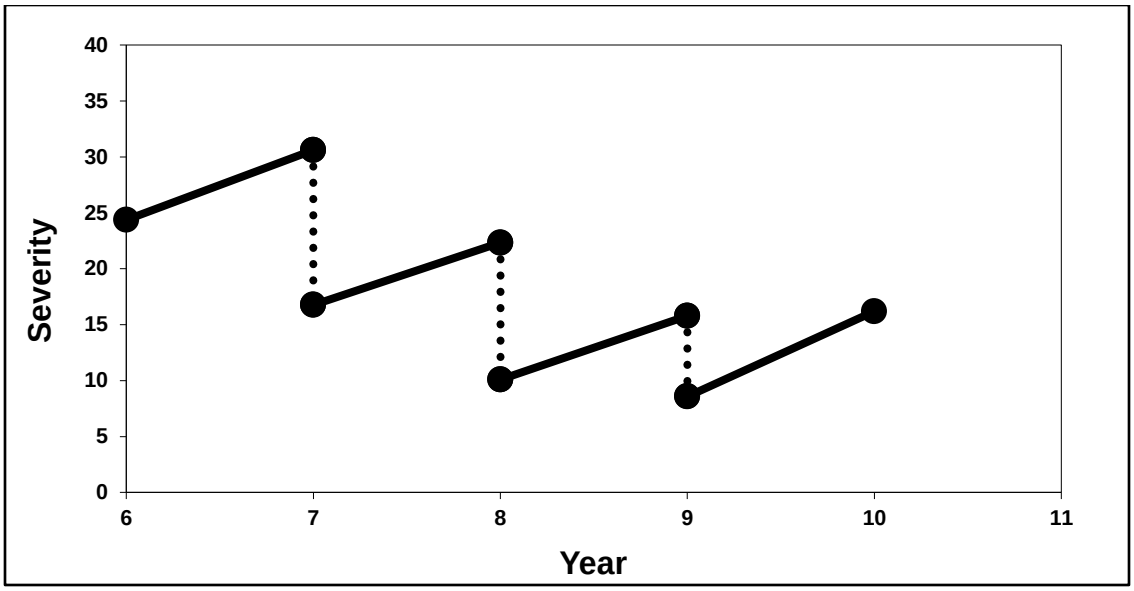

Observed

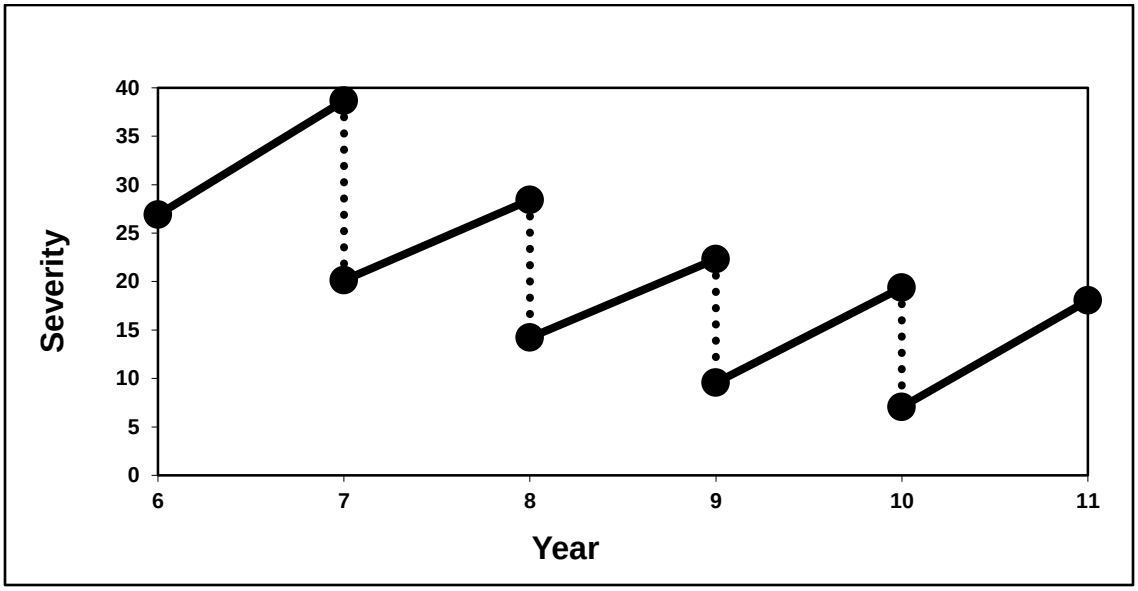

Simulated

Figure 15. Severity of areas with increasing severity ($I_t = 1$) for observed and simulated data. The graph on the top depicts the change of severity of *P. thomsoni* in the Anchorage Bowl, Alaska, with increasing severity of the observed field data from 2006 to 2010. The graph on the bottom depicts the change of severity with increasing severity of the simulated data from 2006 to 2011. Severity is equal to the number of infested leaves out of 50 total leaves examined (Lundquist et al. 2012) , when year = 6 = actual year 2006.

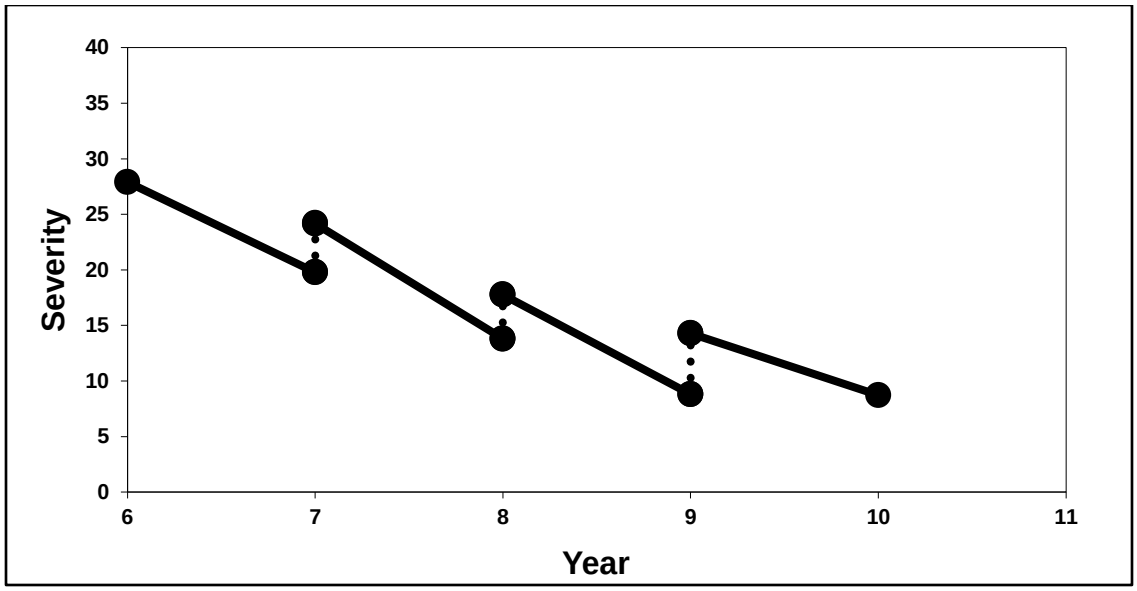

Observed

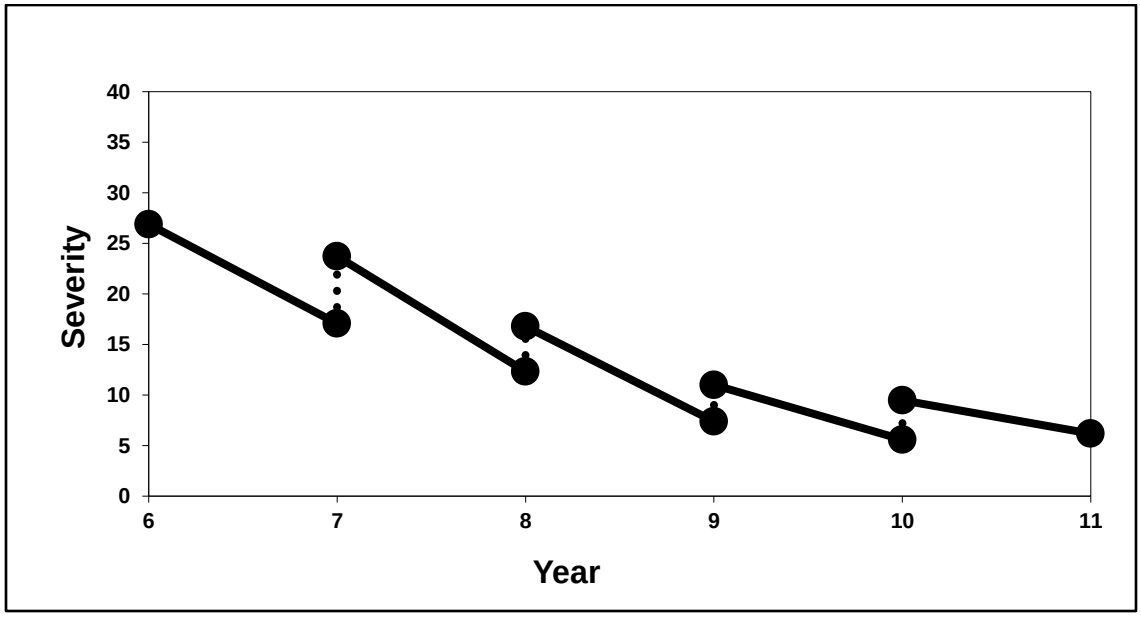

Simulated

Figure 16. Severity of areas with decreasing severity ($I_t = 1$) for observed and simulated data. The graph on the top depicts the change of severity of *P. thomsoni* in the Anchorage Bowl, Alaska, with decreasing severity of the observed field data from 2006 to 2010. The graph on the bottom depicts the change of severity with decreasing severity of the simulated data from 2006 to 2011. Severity is equal to the number of infested leaves out of 50 total leaves examined (Lundquist et al. 2012), when year = 6 = actual year 2006.

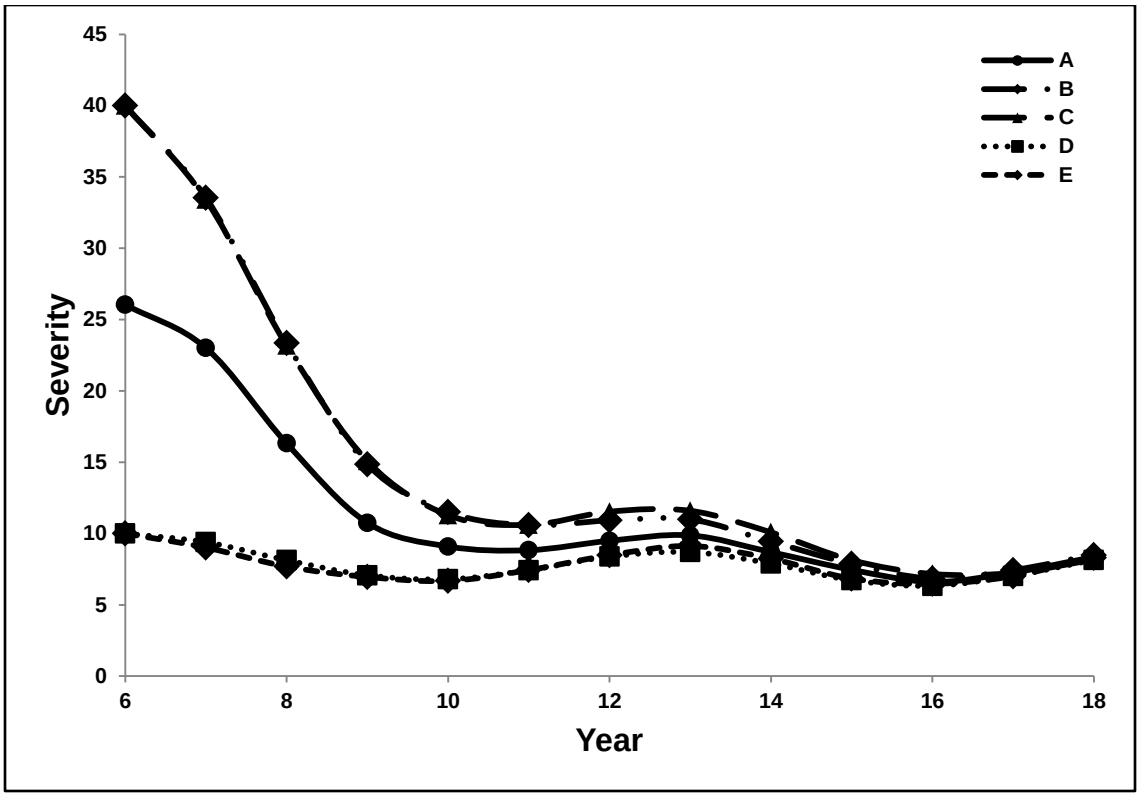

Figure 17. Influence of changing the mean severity and variance in the base year (2006) on the change in severity of *P. thomsoni* from 2000 to 2018 in Anchorage Bowl, Alaska: A) Base Model $\mu = 26.9$, $\sigma^2 = 3$, and CV = $\sigma/\mu = 0.064$, B) Mean = 40, $\sigma^2 = 3$, and CV = 0.043, C) $\mu = 40$; $\sigma^2 = 6.6$, and CV = 0.064, D) $\mu = 10$; $\sigma^2 = 3$, and CV = 0.173, and E) $\mu = 10$; $\sigma^2 = 0.41$, and CV = 0.064, when year = 6 = actual year 2006.

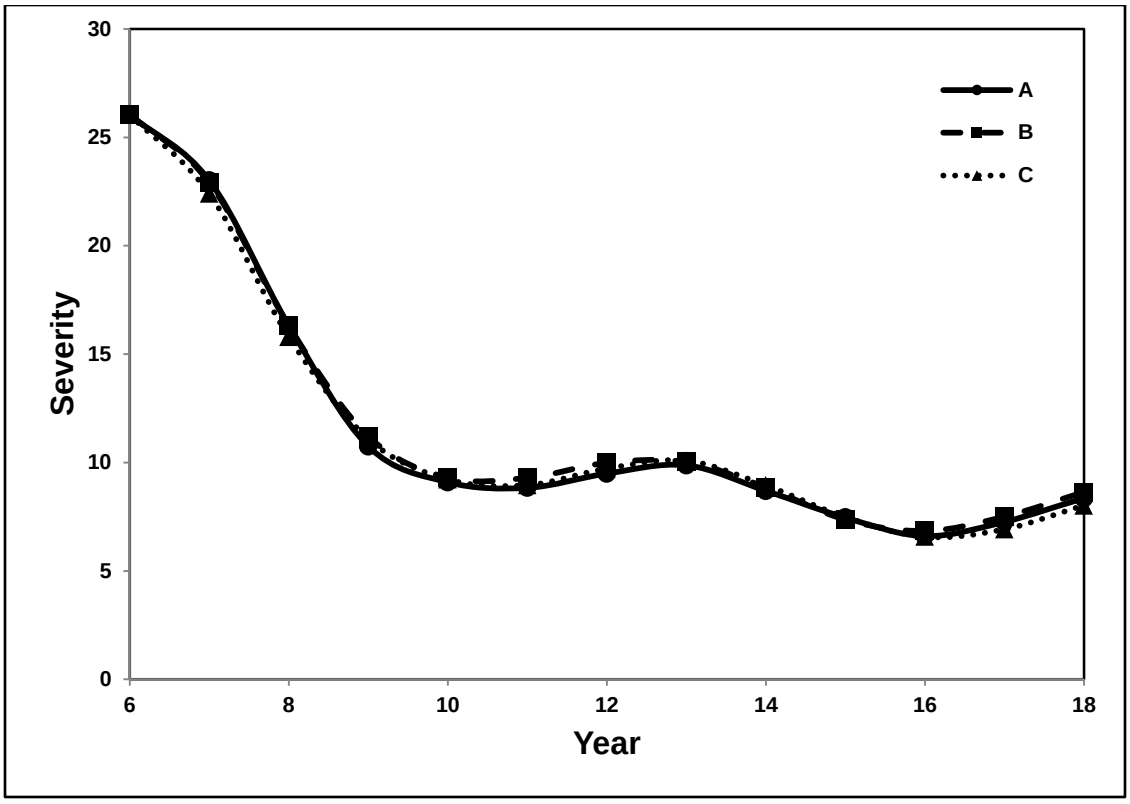

Figure 18. Sensitivity analysis of the random error surface applied to the trend surface model for *P. thomsoni* spread from 2006 -2018 in the Anchorage Bowl, Alaska: A) Simulated Mean (σ^2 = 4), B) σ^2= 8, and C) σ^2 = 2, when year = 6 = actual year 2006.

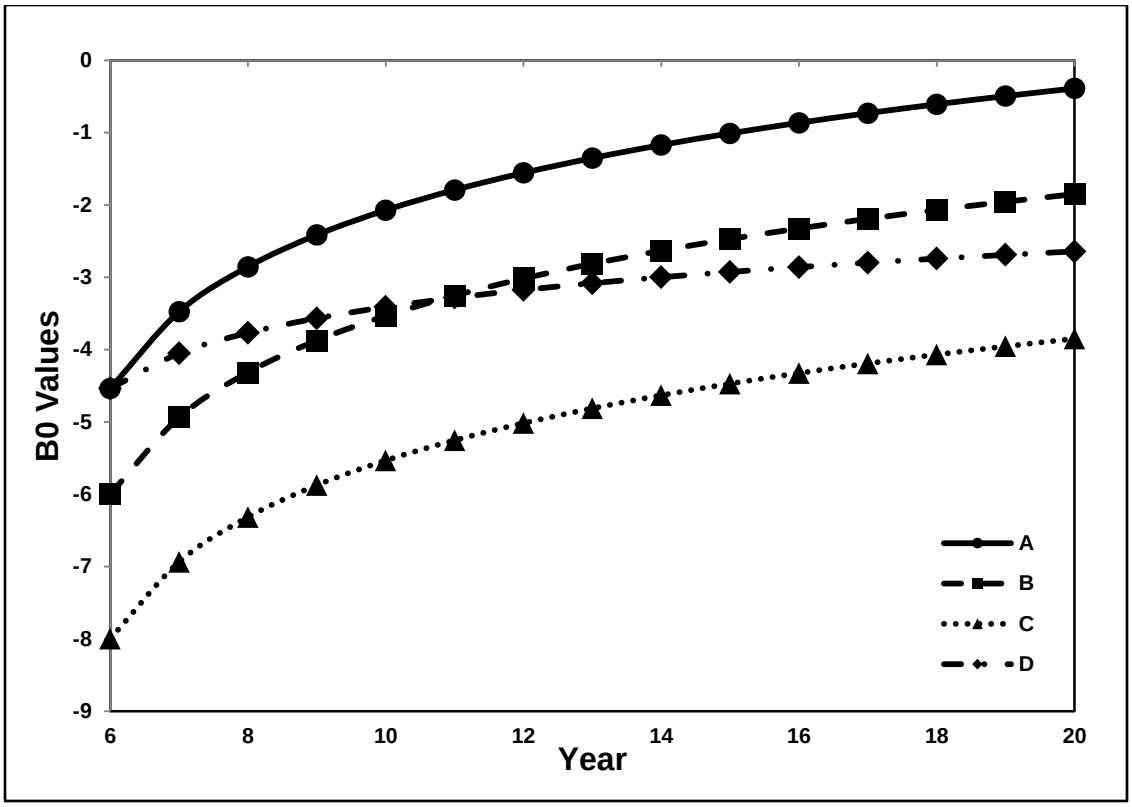

Figure 19. Sensitivity analysis of the trend surface model coefficient $\hat{\beta}_0$ for *P. thomsoni* from 2006 -2018 in the Anchorage Bowl, Alaska: A) Base model $\hat{\beta}_0$ = -4.538418943 + 1.532291784 * ln(t) , B) $\hat{\beta}_0$ = -6.0 + 1.532291784 * ln(t), C) $\hat{\beta}_0$ = -8.0 + 1.532291784 * ln(t), and D) $\hat{\beta}_0$ = -4.538418943 + 0.7 * ln(t); where ln is the natural log, t = time in years, and when year = 6 = actual year 2006; t = 1.

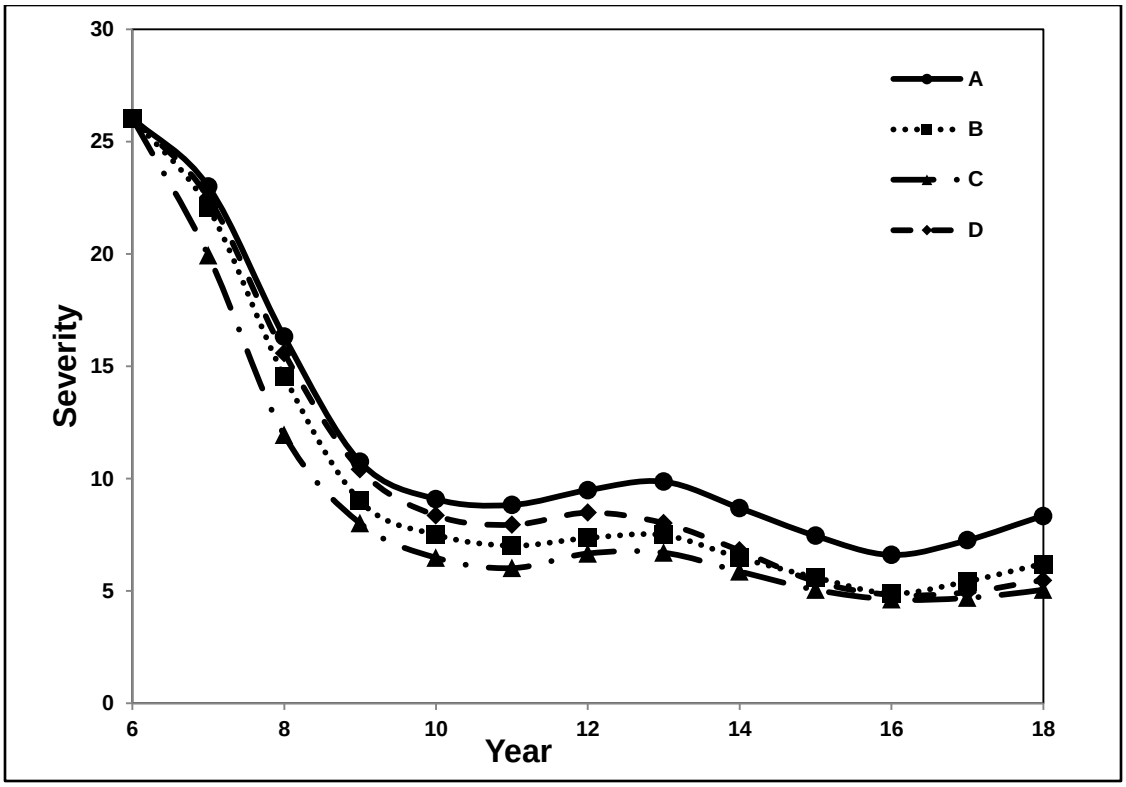

Figure 20. Sensitivity analysis of the trend surface model coefficient $\hat{\beta}_0$ for *P. thomsoni* from 2006 -2018 in the Anchorage Bowl, Alaska: A) Simulated Mean, B) $\hat{\beta}_0$ = -6.0 + 1.532291784 * ln(t), C) $\hat{\beta}_0$ = -8.0 + 1.532291784 * ln(t), and D) $\hat{\beta}_0$ = -4.538418943 + 0.7 * ln(t); where ln is the natural log, t = time in years, and when year = 6 = actual year 2006; t = 1.

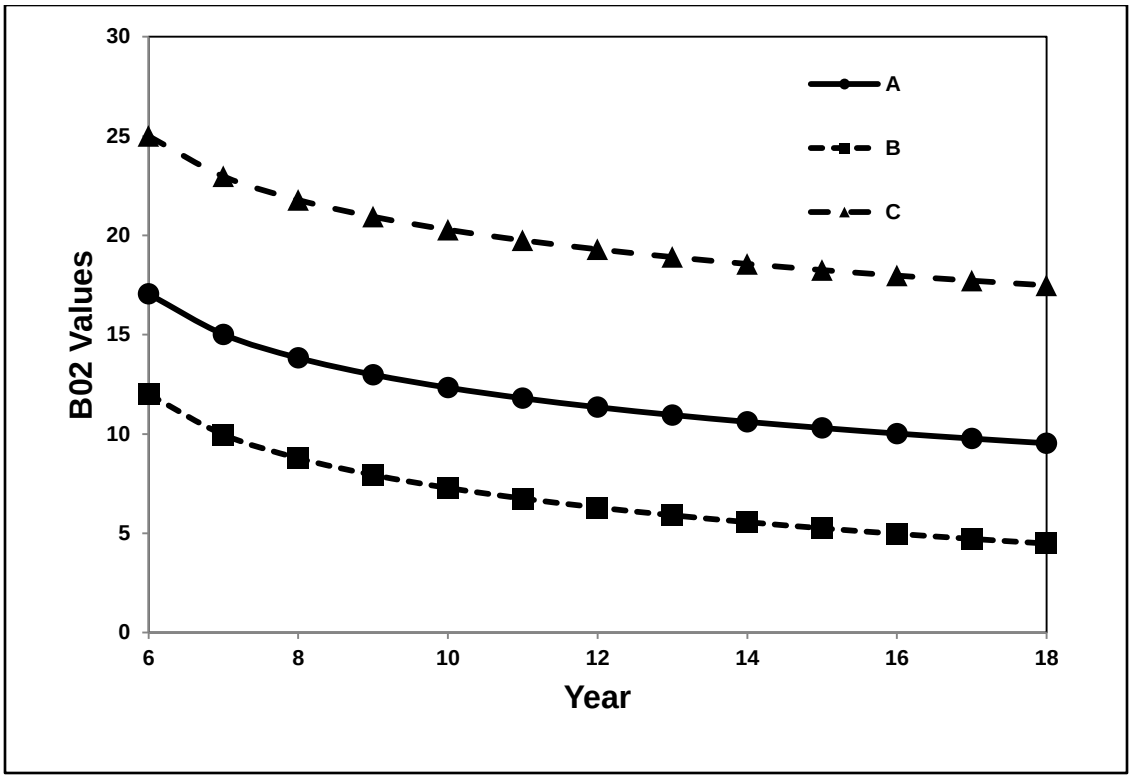

Figure 21. Sensitivity analysis of the trend surface model coefficient $\hat{\beta}_{02}$ for *P. thomsoni* from 2006 -2018 in the Anchorage Bowl, Alaska: A) Base model $\hat{\beta}_{02}$ = 17.04998835 - 2.93085669 * ln(t), B) $\hat{\beta}_{02}$ = 12.0 - 2.93085669 * ln(t), C) $\hat{\beta}_{02}$ = 25.0 - 2.93085669 * ln(t), where $\hat{\beta}_2 = \hat{\beta}_{02} - \hat{\beta}_0$ and ln is the natural log, t = time in years, and when year = 6 = actual year 2006; t = 1.

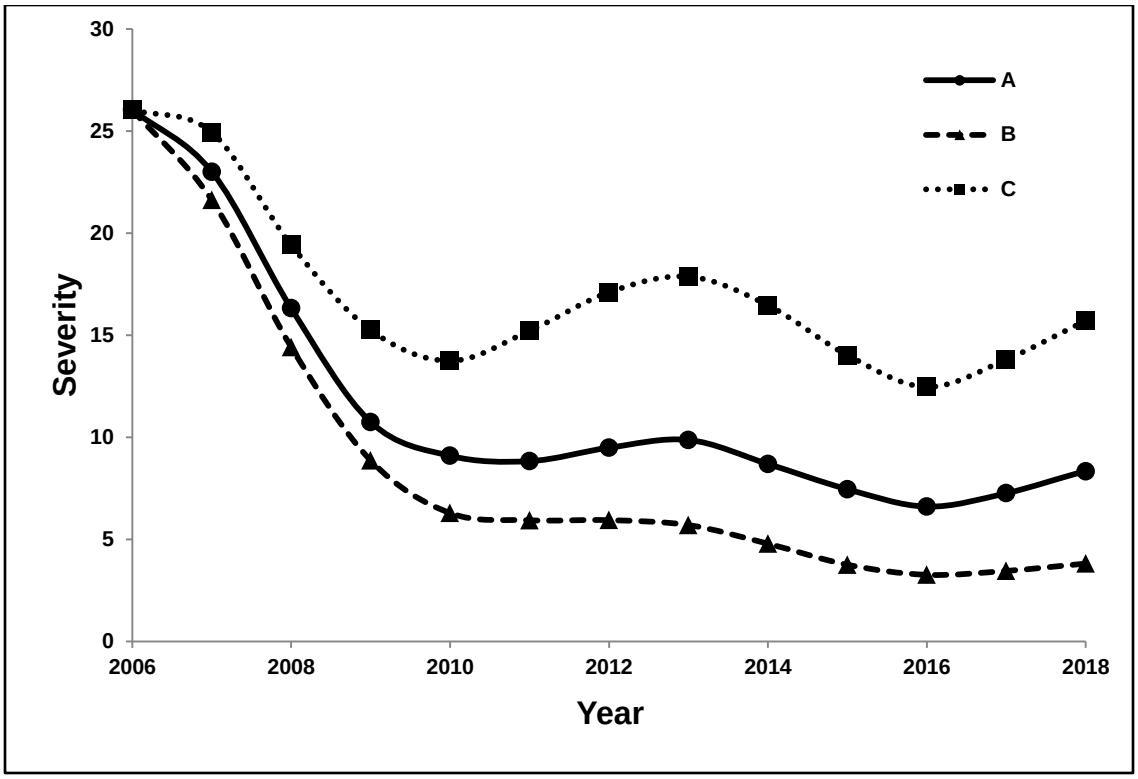

Figure 22. Sensitivity analysis of the trend surface model coefficient $\hat{\beta}_{02}$ for *P. thomsoni* from 2006 -2018 in the Anchorage Bowl, Alaska: A) Simulated Mean, B) $\hat{\beta}_{02}$ = 12.0 + 2.93085669 * ln(t), C) $\hat{\beta}_{02}$ = 25.0 + 2.93085669 * ln(t), where $\hat{\beta}_2 = \hat{\beta}_{02} - \hat{\beta}_0$.

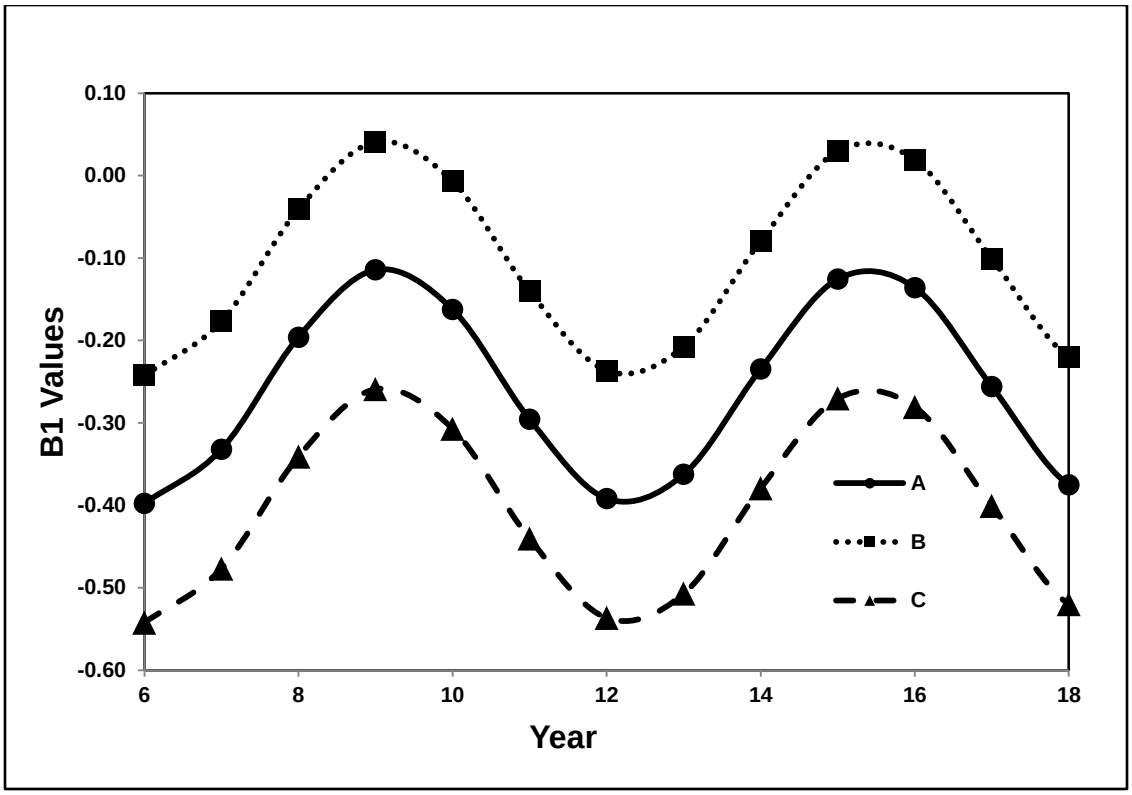

Figure 23. Sensitivity analysis of the trend surface model coefficient $\hat{\beta}_1$ for *P. thomsoni* spread from 2006 - 2018 in the Anchorage Bowl, Alaska: A) Base model $\hat{\beta}_1$ = -0.255196006– 0.142286324 * cos (t-3), B) $\hat{\beta}_1$ = -0.1 – 0.142286324 * cos (t-3), and C) $\hat{\beta}_1$ = -0.4 – 0.142286324 * cos (t-3) , where cos = cosine and t = years (e.g. 2006 = 0 and 2020 = 14).

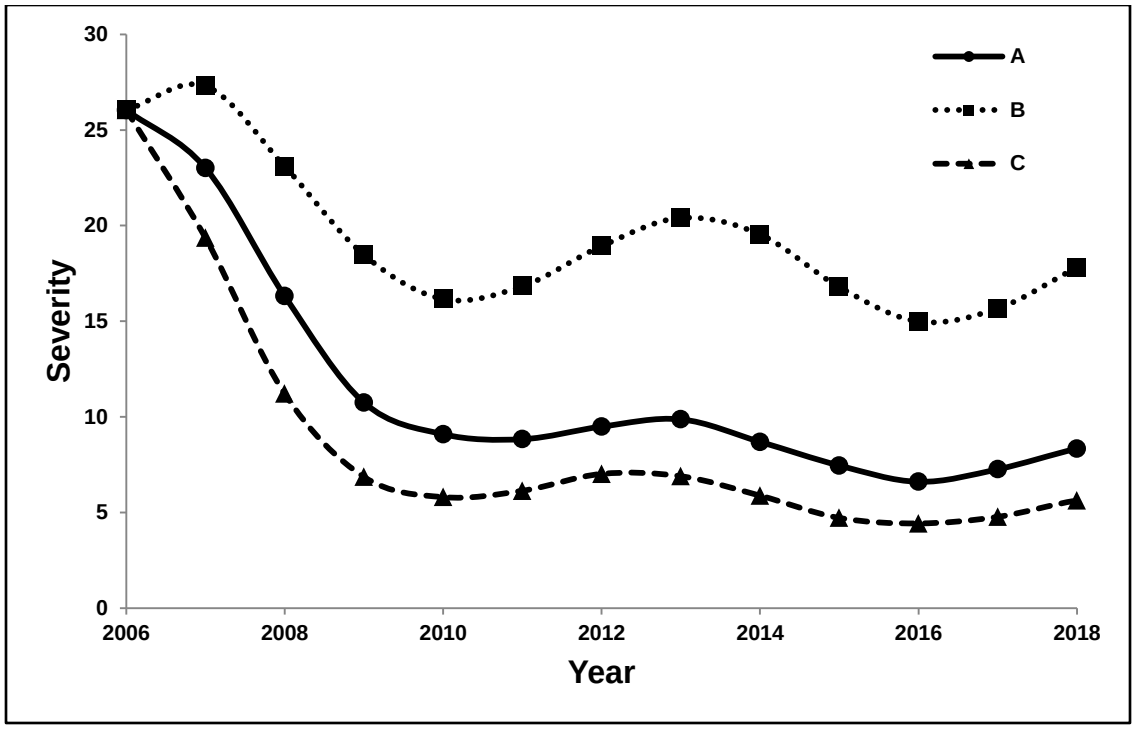

Figure 24. Sensitivity Analysis of the trend surface model coefficient $\hat{\beta}_1$ for *P. thomsoni* from 2006 -2018 in the Anchorage Bowl, Alaska: A) Simulated Mean, B) $\hat{\beta}_1$ = -0.1 – 0.142286324 * cos (t-3), and C) $\hat{\beta}_1$ = -0.4 – 0.142286324 * cos (t-3).

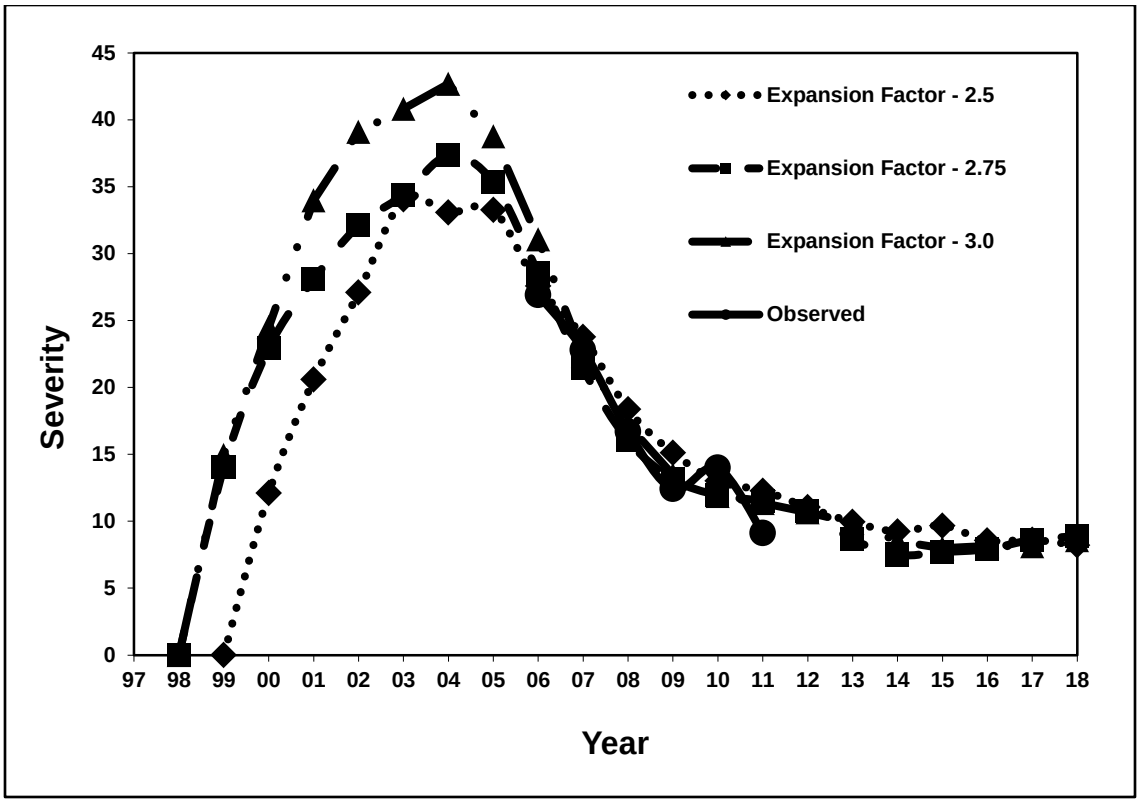

Figure 25. Using hindcasting and forecasting methods to emulate the *P. thomsoni* infestation from the first sighting to 2018. The three scenarios were designed to mimic the first sighting of *P. thomsoni* in 1996 and to match with the observed data in 2006. The three scenarios use a 2.5, 2.75 or 3.0 expansion factor. This graph is the result of 20 simulations.

DISCUSSION

Lundquist et al. (2012) discussed six elements that might help explain the observed spatial and temporal patterns: 1) density-dependent forces, 2) natural enemies, 3) induced resistance, 4) dispersal, 5) spatial heterogeneity and distribution, and 6) multiple causes (a combination of the previously mention factors).

Density-dependent forces could cause areas with high density larval populations to be crowded, such that larvae may compete with each other or become cannibalistic, increasing mortality while decreasing birth rates (MacQuarrie 2008). It is common, especially late in the season, to find two or more larvae sharing a lesion formed when two or more individual blotches coalesced (MacQuarrie 2008). Although *P. thomsoni* has been dominant since birch leaf miners were first monitored in 2006. In 2011 the abundance of *H. nemoratus*, which can often reside on the same leaf, has surpassed *P. thomsoni* abundance (USFS 2011). The role of *H. nemoratus*, and if and how it interacts with *P. thomsoni* may offer insight into the relative importance of density-dependent forces.

Anderson and May (1980, 1981) suggested that cyclic fluctuations of insect populations could be driven by natural enemies. Impacts of fluctuating native predator populations could affect the distribution of *P. thomsoni*. The roles of natural enemies of urban forest insects are considered by many to be significant factors controlling fluctuations and stability of host insect populations (Elton 1927, Andrewartha and Birch 1954). Reeve (1988) coins the term "equilibrium theory" as "the regulation of insect populations about an equilibrium point, by the density-dependent coupling between the insect and its natural enemies…" A massive body of literature has focused on this subject (Dwyer et al. 2000, Dwyer et al. 2004).

The city of Edmonton, Alberta experienced a similar problem with the *P. thomsoni* during the 1970s and 1980s. This nearly 20-year infestation ended with the emergence of a native parasitoid, *Lathrolestes luteolator* (Gravenhorst.), which switched hosts and became parasitic to *P. thomsoni* (Digweed 1998). This parasitoid is credited with decreasing the

population of *P. thomsoni* in Edmonton (Snyder et al. 2007). In 2003, a cooperative consisting of: USDA Forest Service, Canadian Forest Service, and the University of Alberta, began a biological control program featuring the parasitoid *Lathrolestes thomsoni* in Anchorage (Soper 2011).

Changes in tree physiology, which influence susceptibility, could result in delayed induced resistance. Plants defend themselves against herbivory in many ways. These plant defense mechanisms can be classified as constitutive or induced (Lundquist et al. 2012). Constitutive mechanisms are pre-existing chemical or structural barriers that prevent, reduce, or otherwise minimize the impact of a plant feeding insect. Induced mechanisms are stimulated by non-lethal ingress of an herbivore or other source of damage or injury (Karban and Baldwin 1997, Tollrian and Harvell 1998, Agrawal et al. 1999). The induced resistance hypothesis states that plants attacked by insect herbivores are stimulated to produce chemicals that negatively impact the development and growth of the insects. This phenomenon has been examined in several host-insect herbivore systems (Ohgushi 2005), especially birch species (Neuvonen and Niemelä 1991). According to Bryant et al. (1993), delayed induce response is expressed in Alaska paper birch as a prolonged condition of decreased leaf food quality for early instar insect defoliators, smaller leaf size, declining nitrogen levels in leaves, and increasing concentrations of phenolics and other secondary compounds.

One way that insects respond to plant defense mechanisms is to modify feeding behavior (Stamp and Casey 1993) by dispersing to different locations, which could be reflected in the changing spatial distribution of *P. thomsoni*. Dispersal is important for all insect populations at all spatial scales (Sharov 1996). Generally, insect herbivores occupy hosts growing in habitats in which insects and plants are adapted for growth and reproduction. Often, the factors that drive dispersal and the resulting patterns of distribution are difficult to determine. Habitat selection theories (Rosenzweig 1991) and the dynamics of insect populations have been the focus of

countless studies (Sharov 1996), and many population dynamics models have been developed specifically for forest and tree insects (Berryman 1986, Liebhold 1994).

Many studies have found that spatial variation and environmental heterogeneity are significant factors in determining pest distributions (Garvie and Golinski 2010). The application of metapopulation principles to forest entomology is relatively new; however, there seems to be increasing interest in this approach from modelers (Burton and Travis 2008, Goodnight et al. 2008, Sun et al. 2008, Cronin 2009, Han et al. 2009, Mistro et al. 2009, Soubeyrand et al. 2009, Garvie and Golinski 2010). According to Cronin (2009), "movement, and particularly the colonization of new habitat patches, remains one of the least known aspects of the life history and ecology of a vast majority of species."

Natural enemies and plant quality may keep the herbivore population in check. According to Ylioja et al. (1999), "many factors that affect population abundance… can act in either a density dependent or density independent fashion, but the relative contribution of exogenous and endogenous effects remains an open question …" According to Hunter and Price (1992), "The real issue is whether or not we can accept the fact that many ecological factors simultaneously determine the patterns we observe in natural communities (Southwood 1975, 1977b, Quinn and Dunham 1983, Courtney 1988, Leibold 1989), that the dominant forces will vary within and among systems (Karr et al. 1992), and that incorporating and measuring that variability will increase our understanding of population and community ecology."

The spatial heterogeneity expressed by *P. thomsoni* emphasizes the need for spatially explicit studies (Sun et al. 2008). According to Soubeyrand et al. (2009), "…we are usually limited in our ability to investigate the numerical dynamics of natural populations across large spatial scales and over long periods of time." The dynamics that result from interactions between the *P. thomsoni* and its host (Strong et al. 1984), and potential natural enemies (Reeve 1988; 1990), are greatly influenced by this patchy landscape pattern (Comins et al. 1992). Many studies have shown and discussed the importance of patchy environments in promoting sustainable host

populations (Hassell et al. 1991). Reeve (1988) described one possible mechanism for stability in patchy environments: "…insect populations persist because they are divided into a large number of subpopulations, weakly linked by migration; because the subpopulations experience different environments, they are to some extent asynchronous, making the simultaneous extinction of all subpopulations unlikely." From an insect's point of view, spatially asynchronous changes in population density ensure that vulnerable trees are available.

Temporal scales strongly influence insect population distribution. To be successful, short-lived insects that rely on long-lived host must adapt to seasonal variation in host availability (Mopper 2005). The timing of insect life cycles (e.g. egg depositing and larval survival) are closely tied to host quality (Mopper 2005). Therefore, any temporal change in host quality may alter insect populations. Univoltine insects are particularly sensitive to temporal changes in host quality, which can be modified by stressing agents such as drought, extreme temperatures, nutrient depletion, or defoliation.

Model

A Cellular Automata (CA) model was developed to emulate the spatial and temporal spread of *P. thomsoni* in the Anchorage Bowl, Alaska. The CA model contains implied density-dependent factors, plant defenses, and natural enemies interacting. The density-dependent factors and plant defenses are stochastic processes influencing the severity and the spatial and temporal distribution of the areas of random size and shape. Liebhold and Tobin (2008) and Schofield (2002) discuss two population bounds (i.e. a minimum and maximum). The first bound is carrying capacity and it is a maximum population size. The second bound is a minimum and is called the Allee effect (Allee 1927, Schofield 2002, Liebhold and Tobin 2008, Richter et al. 2012). When a population exceeds carrying capacity, it will decrease in size due to density-dependent factors. In addition, when a population approaches carrying capacity, the number of natural enemies may also increase, thereby increasing predation. If the population decreases

below the minimum (Allee effect) value, the population will become extinct. The Allee effect is such that a decrease in population is related to a decrease rate in the number of insects produced. Therefore, if the population is to remain viable, it must be greater than the Allee effect and less than carrying capacity. The Allee effect can be the result of multiple causes, including the lack of cooperative feeding (Liebhold and Tobin 2008), natural enemies (Petrovskii et al. 2002), and plant defenses among others.

Based on the results of this study, we hypothesize that three phases to the *P. thomsoni* infestation occurred in the Anchorage Bowl: 1) expansion, 2) decline, and 3) equilibrium. From the years 1998 to 2004, *P. thomsoni* population expanded, during which time, plant defenses might have been low or nonexistent possibly because the trees had not previously been exposed to *P. thomsoni*. From 2005 to 2011, *P. thomsoni* was in overall decline, possibly triggered first by density-dependent factors coupled with an abundance of natural enemies, followed by an increase in plant defenses. From 2011 to 2018, the population of *P. thomsoni* stabilized and reached equilibrium.

Expansion Phase

During the expansion phase, disjointed regions with high severity levels of infestation were randomly moving about the landscape from year to year. The expansion phase spanned approximately six years, during which most of the study area experiences some level of infestation.

Insect invasions are regulated by available host, carrying capacity (density-dependent factors), and the existing predator population numbers. Large quantities of host trees were available in the study area. Also, *P. thomsoni* is an invasive insect in the Anchorage Bowl; hence, the likelihood of an existing natural predator within the study area was low. In addition, the transportation of adult insects via automobile from heavily infested areas to new locations

possibly exacerbated the expansion (Snyder et al. 2007). Consequently, the *P. thomsoni* infestation expanded throughout the study area.

It is highly likely that during the six year expansion phase, plant defenses were building in intensity over the entire study area. Furthermore, the population of *P. thomsoni* was most likely approaching carrying capacity. A similar expansion phase of *P. thomsoni* was observed in Alberta, Canada in the early 1980's (Snyder et al. 2007).

Declining Phase

After the six year expansion phase, the declining phase began. This phase can be described as the change in severity that decreases at an increasing rate. The possible driving forces for this phase may be the combination of density-dependent factors, natural enemies, and to a lesser extent plant defenses.

As the numbers of larvae infesting a single leaf at a single point in time increase, insect mortality due to competition for resources and or cannibalism may occur (Liebhold and Tobin 2008, MacQuarrie et al. 2010, Lundquist et al. 2012) . Therefore, as the numbers of pupae die in the current year due to the density-dependent factors, the insect population numbers in the next year will subsequently be lower.

Two other invasive sawflies late birch leaf edge miner (*Heterarthrus nemoratus*) and birch leaf miner (*Fenusa pusilla* Lepeletier) were found in the Anchorage Bowl. These two sawflies directly compete with *P. thomsoni* for resources. Snyder et al. (2007) measured the relative abundance of these two sawflies from 2003 to 2005. The results indicated that abundance levels were very low for 2003 and 2004. In 2005, the abundance of these two sawflies increased. In 2011 *H. nemoratus* became the most abundant saw fly in Anchorage (USFS 2011)

The parasitoid (*L. luteolator*) is a predator of *P. thomsoni* (Digweed 1998). Some simple predator-prey relationships exhibit a simple harmonic function shifted by some uniform time period. For example, as the prey population increases in an area, so does the population of

predators; however, the predator population growth rate usually lags by a time period. As the prey population decreases due to predation, the predator population also declines with a temporal lag. Moreover, predator-prey relationships often follow a Lotka-Volterra like model. Essentially, the parasitoid population can follow the infestation groups of *P. thomsoni*, which increased in severity over the landscape in the Anchorage Bowl with at least a one-year time lag. Petrovskii et al. (2002) states that an insect invasion can take the form of irregular shaped patches distributed over the landscape under a predator-prey system.

L. luteolator was introduced on an annual basis as a biological control method in the Anchorage Bowl from 2004 to 2006 (Snyder et al. 2007). From 2006 to 2009 another parasitoids *Lathrolestes thomsoni* was released in Anchorage (Soper 2011). The research by Soper (2011) showed that in 2006 and 2007 two other native parasitoids *Lathrolestes soperi* (Reshchikov et al. 2010) and *Aptesis segnis* were identified as population regulators of *P. thomsoni* in Anchorage. Soper (2011) presumes that the decline of *P. thomsoni* in Anchorage from 2006 – 2011 is due in part to these parasitoids (*L. soperi*, *L. thomson*, and *A. segnis*).

After one season of heavy defoliation, the trees can produce defenses in the form of either constitutive, induced, or both. These plant defenses can influence overall host quality. Many researchers have discussed host quality (Bryant et al. 1993, Hoch et al. 2000, Haukioja 2005, Sisterson 2008, Hatcher et al. 2012) and how it can influence insect population dynamics.

A constitutive plant defense is an increase in the amounts of chemical compounds such as phenols, terenoids, and alkaloids in the leaf tissue in the following year after defoliation. Haukioja (2005) states that defoliation can change plant alleliochemistry, cell structure, and overall plant physiology. The increase in these compounds may make the foliage unpalatable to pests. Alternatively, the tree may produce lower levels of proteins and water in the foliage, which reduces the nutrient-resource content in the leaves. This makes the foliage less nutritious and can negatively influence the insects population dynamics (Haukioja 2005). Bryant et al. (1993) investigated delayed induce resistance in Alaska paper birch. One finding of this Bryant et al.

(1993) experiment was that the plants respond to defoliation via a decline in the nutritional quality of leaves for immature insects for up to three years after defoliation.

An induced process of defoliation can have cascading effects on soil chemistry (Kosola et al. 2001). The reduction of leaf organic material due to insect herbivory affects soil carbon to nitrogen (C:N) ratios which regulate soil microbial activity and population size (Tisdale et al. 1985). Soil microbial activity influences the available nitrogen to plants. Over time, most forest soils have developed a stable C:N ratio. Generally, leaf materials from a tree in a forest landscape have a narrow C:N ratio (approximately 30: 1) (Brady 1974). Therefore, defoliation of the forest canopy reduces leaf material and possibly widens the C:N ratio (i.e. 50:1) of soil litter inputs. The net annual reduction of nitrogen inputs causes the soil microorganisms to deplete stores of nitrogen in the soil (i.e. nitrogen immobilization) and in tree roots (Tisdale et al. 1985). Depleting the soil nitrogen causes mortality of mycorrhizal fungi (Kosola et al. 2001), which causes the death or lack of growth of tree roots. The reduction in tree root growth possibly lowers nutrients in next year's leaf production, thereby reducing overall host quality.

Equilibrium Phase

After the declining phase has run its course, the equilibrium phase occurs. This state can be described as the tree exerts just enough pressure via plant defenses to keep the insect population in check. The insect population size is positioned such that it is slightly greater than the Allee effect point and much less than carrying capacity. This point is also shown in the research done by Hatcher et al. (2012) where, as host quality decreases, the number of parasite feeding on that host also decreases. It is also likely that parasitoids play a minor role in maintaining long term equilibrium. It is also likely that low, stabilized population levels of *P. thomsoni* can be found in Alberta, Canada.

In the birch forest of Europe, *P. thomsoni* populations exist in equilibrium. No research has been done on *P. thomsoni* populations in Europe. Therefore, it is not known if the population

of *P. thomsoni* ever exceeded carrying capacity at some point in the past and crashed. However, it is known and documented that *P. thomsoni* reached large numbers in Alberta, Canada in the 1980s (Snyder et al. 2007). No study was conducted on the population densities or severity of *P. thomsoni* in Alberta during this time period. In the early 1990s, the *P. thomsoni* population crashed in Alberta.

Spread

The spread of some insect populations is akin to a moving-wave front (Yemshanov et al. 2009, Richter et al. 2012). However, if the population is in a declining phase; thus, reducing in numbers, then the moving-wave front may reverse (Schofield 2002). However, the *P. thomsoni* infestation is not a moving wave; rather, a series of random areas of size and shape, erupting in intensity within the study area. The possible forces that drive the spatial distribution of the random areas of size and shape and the severity of the infestation in the Anchorage Bowl are density-dependent factors, plant defenses, and parasitoids. Therefore, if the areas of random size and shape are reducing in severity as illustrated in the declining phase; then, the expansion phase may be reversed.

The lack of density-dependent factors, plant defenses, and natural enemies may lead to the expansion phase. The density-dependent factors, natural enemies, and to a lesser extent plant defenses are potential rapid response forces which may lead to the declining phase. Finally, plant defenses are believed to be the primary long-term force; while, natural enemies are a weaker force in maintaining the equilibrium phase.

CONCLUSION

A Cellular Automata (CA) model was developed to emulate the spatial and temporal spread of *P. thomsoni* in the Anchorage Bowl, Alaska from 1998 to 2018. The CA model uses the severity in the previous year coupled with areas of random size and shape moving about the landscape to model future severity.

The model closely mimics the observed data. The population of *P. thomsoni* has been on a decline since 2006. It is likely that the population of the *P. thomsoni* will remain at low, stabilized levels for an extended period of time in the Anchorage Bowl. This level will be slightly above the Allee effect and well below carrying capacity. This is possibly what occurred in the *P. thomsoni* native European forest and in Alberta, Canada.

In summary, plant defenses are possible long-term cyclic force, manipulating the severity of *P. thomsoni* in the Anchorage Bowl. In addition, density-dependent factors and the parasitoids are possible rapid, cyclic, and short-term modifiers of the *P. thomsoni* population in the Anchorage Bowl.

REFERENCES

Agrawal, A. A., S. Tuzun, and E. Bent. 1999. Induced plant defenses against pathogens and herbivores: biochemistry, ecology, and agriculture. APS Press, St. Paul. MN, USA.

Allee, W. C. 1927. Animal Aggregation. Quarterly Review of Biology 2:367-398.

Anderson, R. M. and R. M. May. 1980. Infectious diseases and population-cycles of forest insects. Science 210:658-661.

Anderson, R. M. and R. M. May. 1981. The population dynamics of microparasites and their invertebrate hosts. Philosophical Transactions of the Royal Society of London, Biological Sciences 291:451-524.

Andrewartha, H. G. and L. C. Birch. 1954. The distribution and abundance of animals. Chicago University Press, Chicago, IL, USA.

Atkinson, P. M. and A. R. L. Tatnall. 1997. Neural networks in remote sensing - Introduction. International Journal of Remote Sensing 18:699-709.

Bauer, A. L., C. A. A. Beauchemin, and A. S. Perelson. 2009. Agent-based modeling of host-pathogen systems: The successes and challenges. Information Sciences 179:1379-1389.

Benson, R. B. 1959. Further studies on the Fenusini (Hymenoptera:Tenthredinidae). Proceedings of the Royal Entomological Society of London Series B 28:90-92.

Berlekamp, E. R., J. H. Conway, and R. K. Guy. 2003. Winning ways for your mathematical plays. 2nd. AK Peters, Ltd, Natick, Massachusetts, USA.

Berryman, A. 1986. Forest Insects: Principles and Practice of Population Management Plenum Press, New York, New York, USA.

Bian, L. and D. Liebner. 2005. Simulating Spatially Explicit Networks for Dispersion of Infectious Diseases. Page 480 *in* D. J. Maguire, M. Batty, and M. F. Goodchild, editors. GIS, Spatial Analysis, and Modeling. ESRI Press, Redlands, CA, USA.

Brady, N. C. 1974. The Nature and Property of Soils. 8th edition. Macmillan Publishing, New York, New York, USA.

Bryant, J. P., P. B. Reichardt, T. P. Clausen, and R. A. Werner. 1993. Effects of mineral nutrition on delayed inducible resistance in Alaska paper birch. Ecological Society of America 74:2072 - 2084.

Burton, O. J. and J. M. J. Travis. 2008. Landscape structure and boundary effects determine the fate of mutations occurring during range expansions. Heredity 101:329-340.

Campos, D., V. Mendez, and V. Ortega-Cejas. 2008. Lattice models for invasions through patchy environments. Bulletin of Mathematical Biology 70:1937-1956.

Chan, W. K. V., S. Young-Jun, and C. M. Macal. 2010. Agent-Base Simulation Tutorial - Simulation of Emergent Behavior and Differences Between Agent-Based Simulation and Discrete-Event Simulations.

Comins, H. N., M. P. Hassell, and R. M. May. 1992. The spatial dynamics of host-parasitoid systems Journal of Animal Ecology 611:735-748.

Courtney, S. P. 1988. If it's not coevolution, it must be predation. Ecology 69:910-911.

Cronin, J. T. 2009. Movement, colonization, and establishement success of a planthopper of prairie poteholes, Delphacodes scolochloa (Hemiptera: Delphacidae). Ecologcial entomology 34:114-124.

Deadman, P., D. Robinson, E. Moran, and E. Brondizio. 2004. Colonist household decisionmaking and land-use change in the Amazon Rainforest: an agent-based simulation. Environment and Planning B-Planning & Design 31:693-709.

DeRose, R. J. and J. N. Long. 2012. Factors Influencing the Spatial and Temporal Dynamics of Engelmann Spruce Mortality during a Spruce Beetle Outbreak on the Markagunt Plateau, Utah. Forest Science 58:1-14.

Digweed, S. C. 1998. Mortality of birch leafmining sawflies (Hymenoptera : Tenthredinidae): Impacts of natural enemies on introduced pests. Environmental Entomology 27:1357-1367.

Digweed, S. C. 2006. Oviposition preference and larval performance in the exotic birch-leafmining sawfly Profenusa thomsoni. Entomologia Experimentalis Et Applicata 120:41-49.

Digweed, S. C. and D. W. Langor. 2004. Distributions of leafmining sawflies (Hymenoptera : Tenthredinidae) on birch and alder in northwestern Canada. Canadian Entomologist 136:727-731.

Digweed, S. C., C. J. K. MacQuarrie, D. W. Langor, D. J. M. Williams, J. R. Spence, K. L. Nystrom, and L. Morneau. 2009. Current status of invasive alien birch-leafmining sawflies (Hymenoptera: Tenthredinidae) in Canada, with keys to species. Canadian Entomologist 141:201-235.

Digweed, S. C., R. L. McQueen, J. R. Spence, and D. W. Langor. 2003. Biological Control of the Ambermarked Birch Leafminer, Profenusa thomsoni (Hymenoptera: Tenthredinidae), in Alberta. Northern Forestry Centre Information Report NOR-X-389. Natural Resources Canada, Canadian Forest Service, Edmonton, Alberta. National Library of Canada cataloguing in publication data, Canada.

Dwyer, G., J. Dushoff, J. S. Elkinton, and S. A. Levin. 2000. Pathogen-driven outbreaks in forest defoliators revisited: building models from experimental data. The American Naturalist 156:105-120.

Dwyer, G., J. Dushoff, and S. Yee. 2004. The combined effects of pathogens and predators on insect outbreaks. Nature 430:341-345.

Elton, C. 1927. Animal Ecology. Sidgwick Jackson, London, UK.

ESRI. 2007. U.S. Populated Place Areas.*in* ESRI, editor. ESRI, Redland, California.

Fisher, R. 1937. The wave of advance of an advantageous gene. Annuals. Eugenics 7:353–369.

Garvie, M. R. and M. Golinski. 2010. Metapopulation dynamics for spatially extended predator-prey interactions. Ecological Complexity 7:55-59.

Goldstein, M., D. Martin, B. Schrader, P. Hennon, E. Holsten, and J. Kruse. 2005. Assessment of invasives species in Alaska and its national forest. USDA Forest Service Assessment Report, Anchorage, AK.

Goodnight, C., E. Rauch, H. Sayama, M. A. M. De Aguiar, M. Baranger, and Y. Bar-Yam. 2008. Evolution in spatial predator-prey models and the "Prudent predator": The inadequacy of steady-state organism fitness and the concept of individual and group selection. Complexity 13:23-44.

Han, Q., X. F. Liao, and C. D. Li. 2012. Complex Dynamic Behaviors in Cellular Automata Rule 14. Discrete Dynamics in Nature and Society.

Han, X. Z., C. Hui, and Y. Y. Zhang. 2009. Effects of time-lagged niche construction on metapopulation dynamics and environmental heterogeneity. Applied Mathematics and Computation 215:449-458.

Hartley, S., P. D. Krushelnycky, and P. J. Lester. 2010. Integrating physiology, population dynamics and climate to make multi-scale predictions for the spread of an invasive insect: the Argentine ant at Haleakala National Park, Hawaii. Ecography 33:83-94.

Hassell, M. P., R. M. May, S. W. Pacala, and P. L. Chesson. 1991. The Persistence of Host-Parasitoid Association in Patchy Environments .1. A General Criterion. American Naturalist 138:568-583.

Hatcher, M. J., J. T. A. Dick, and A. M. Dunn. 2012. Diverse effect of parasites in ecosystems: linking interdependent processes. Fontiers in Ecology and the Environment 10:186 - 193.

Haukioja, E. 2005. Plant defenses and population fluctuations of forest defoliators: mechanism-based scenarios. Annales Zoologici Fennici 42:313-325.

Haynes, K. J., A. M. Liebhold, and D. M. Johnson. 2009. Spatial analysis of harmonic oscillation of gypsy moth outbreak intensity. Oecologia 159:249-256.

Hoch, W. A., E. L. Zeldin, and B. H. McCown. 2000. Resistance to the birch leafminer Fenusa pusilla (Hymenoptera : Tenthredinidae) within the genus Betula. Journal of Economic Entomology 93:1810-1813.

Huang, H. M., L. Q. Zhang, Y. J. Guan, and D. H. Wang. 2008. A cellular automata model for population expansion of Spartina alterniflora at Jiuduansha Shoals, Shanghai, China. Estuarine Coastal and Shelf Science 77:47-55.

Hunter , M. and P. W. Price 1992. Playing chutes and ladders: heterogeneity and the relative roles of bottom-up and top-down forces in natural communities. Ecology 73:724 – 732.

Jeger, M. J., M. Pautasso, O. Holdenrieder, and M. W. Shaw. 2007. Modelling disease spread and control in networks: implications for plant sciences. New Phytologist 174:279 - 297.

Karban, R. and I. T. Baldwin. 1997. Induced responses to herbivory. University of Chicago Press, Chicago, IL, USA

Karr, J. R., M. Dionne, and I. J. Schlosser. 1992. Bottom- up versus top-down regulation of vertebrate populations: lessons from birds and fish. Pages 243-286 *in* M. D. Hunter, T. Ohgushi, and P. W. Price, editors. Effects of resource distribution on animal-plant interactions. Academic Press, San Diego, California, USA.

Kosola, K. R., D. I. Dickmann, E. A. Paul, and D. Parry. 2001. Repeated insect defoliation effects on growth, nitrogen acquisition, carbohydrates, and root demography of poplars. Oecologia 129:65-74.

Leibold, M. A. 1989. Resource edibility and the effects of predators and productivity on the outcome of trophic interactions. American Naturalist 134:922-949.

Liebhold, A. and N. Kamata. 2000. Introduction - Are population cycles and spatial synchrony a universal characteristic of forest insect populations? Population Ecology 42:205-209.

Liebhold, A. M. 1994. Use and abuse of insect and disease models in forest pest management: past, present, and future., USDA Forest Service.

Liebhold, A. M., J. A. Halverson, and G. A. Elmes. 1992. Gypse moth invasion in North America: a quantitative analysis. Journal of Biogeography 19:513 - 520.

Liebhold, A. M. and P. C. Tobin. 2008. Population ecology of insect invasions and their management. Annual Review of Entomology 53:387-408.

Lundquist , J. E., R. M. Reich, and M. Tuffly. 2012. Spatial dynamics of the invasive defoliator Amber-marked birch leaf miner (*Profesusa thomsoni*) across the Anchorage landscape. Journal of Economic Entomology 105:1659 - 1667.

MacQuarrie, C. J. K. 2008. Invasion history, population dynamics and biological control of Profenusa thomsoni (Konow) in Alaska University of Alberta, Alberta Canada.

MacQuarrie, C. J. K., J. R. Spence, and D. W. Langor. 2010. Using classification tree analysis to reveal causes of mortality in an insect population. Agricultural and Forest Entomology 12:143-149.

Mathey, A. H., E. Krcmar, S. Dragicevic, and I. Vertinsky. 2008. An object-oriented cellular automata model for forest planning problems. Ecological Modelling 212:359-371.

Mercader, R. J., N. W. Siegert, A. M. Liebhold, and D. G. McCullough. 2009. Dispersal of the emerald ash borer, Agrilus planipennis, in newly-colonized sites. Agricultural and Forest Entomology 11:421-424.

Mercader, R. J., N. W. Siegert, A. M. Liebhold, and D. G. McCullough. 2011. Influence of foraging behavior and host spatial distribution on the localized spread of the emerald ash borer, Agrilus planipennis. Population Ecology 53:271-285.

Mistro, D. C., L. D. D. Rodrigues, and M. C. Varriale. 2009. The role of spatial refues incoupled map lattice model for host-parasitoid systems. Bulletin of Mathematical Biology 71:1934-1953.

Mopper, S. 2005. Phenology - how time creates spatial structure in endophagous insect populations. Annales Zoologici Fennici 42:327-333.

Morin, R. S., A. M. Liebhold, and K. W. Gottschalk. 2009. Anisotropic spread of hemlock woolly adelgid in the eastern United States. Biological Invasions 11:2341-2350.

Neuvonen, S. and P. Niemelä. 1991. Do differences in inducible resistance explain the population dynamics of birch and pine defoliators? , USDA Forest Service, USA.

Ohgushi, T. 2005. Indirect Interaction Webs: Herbivore-Induced Effects Through Trait Change in Plants. Annual Review Ecology Evolution Systems 36:81 - 105.

Perez, L. and S. Dragicevic. 2012. Landscape-level simulation of forest insect disturbance: Coupling swarm intelligent agents with GIS-based cellular automata model. Ecological Modelling 231:53-64.

Petrovskii, S. V., A. Y. Morozov, and E. Venturino. 2002. Allee effect makes possible patchy invasion in a predator-prey system. Ecology Letters 5:345-352.

Quinn, J. F. and A. E. Dunham. 1983. On hypothesis testing in ecology and evolution. American Naturalist 122:602- 617.

R Development Core Team. 2008. *R: A lanuage and environment for stastical computing*. R Foundation for Statistical Computing, Vienna, Austria.

Rasmussen, R. and G. Hamilton. 2012. An approximate Bayesian computation approach for estimating parameters of complex environmental processes in a cellular automata. Environmental Modelling & Software 29:1-10.

Reeve, J. D. 1988. Environmental variability, migration, and persistence in host-parasitoid systems. American Naturalist 132:810-836.

Reshchikov, A. V., A. L. Soper, and R. G. Van Driesche. 2010. Review and key to Nearctic Lathrolestes Förster (Hymenoptera: Ichneumonidae), with special reference to species attacking leaf mining tenthredinid sawflies in Betula Linnaeus (Betulaceae). Zootaxa 2614:1 - 17.

Reynolds, C. W. 1987. Flocks, herds, and schools: A distributed behavioral model. SIGGRAPH '87. Computer Graphics (ACM) 21:25-34.

Richter, O., S. Moenickes, and F. Suhling. 2012. Modelling the effect of temperature on the range expansion of species by reaction-diffusion equations. Mathematical Biosciences 235:171-181.

Rosenzweig, M. L. 1991. Habitat selection and population interactions: the search mechanism. . American Naturalist 137:S5-S28.

Schlather, M. 2012. Simulation and Analysis of Random Fields. Page Simulation of Gaussian and extreme value random fields; conditional simulation; kriging *in* M. Schlather, editor. Simulation and Analysis of Random Fields, Germany.

Schofield, P. 2002. Spatially explicit models of Turelli-Hoffmann Wolbachia invasive wave fronts. Journal of Theoretical Biology 215:121-131.

Sharov, A. A. 1996. Modeling Insect Dynamics. Caring for the forest: research in a changing world, Congress report Vol II. IUFRO XX World Congress edition. World Congress, Tampere, Finland.

Sisterson, M. S. 2008. Effects of insect-vector preference for healthy or infected plants on pathogen spread: Insights from a model. Journal of Economic Entomology 101:1-8.

Snyder, C., C. J. K. MacQuarrie, K. Zogas, J. J. Kruse, and J. Hard. 2007. Invasive species in the last frontier: Distribution and phenology of birch leaf mining sawflies in Alaska. Journal of Forestry 105:113-119.

Soper, A. 2011. Success Story: Amber-Marked Birch Leaf Miner Biological Control. USFS Alaska Region R10 PR 25 and State of Alaska Department of Natural Resources Division of Forestry Accessed on October 25, 2012. http://www.fs.usda.gov/Internet/FSE_DOCUMENTS/stelprdb5360665.pdf,

Soper, A., R. V. Driesche, and C. MacQuarrie. 2009. Biological Control of Pests in Forests of Eastern United States. UMassAmherst. Accessed on October 25, 2012. http://www.invasiveforestinsectandweedbiocontrol.info/target_pests/insects_mites/amblm.htm.

Soubeyrand, S., A. L. Laine, I. Hanski, and A. Penttinen. 2009. Spatiotemporal structure of host pathogen interactions in a metapopulation. American Naturalist 174:308-320.

Southwood, T. R. E. 1975. The dynamics of insect populations. Academic Press, New York, New York, USA.

Southwood, T. R. E. 1977b. The relevance of population dynamics theory to pest status *in* J. M. Cherret and G. R. Sagar, editors. Origins of pest, parasite, disease and weed problems. Symposium of the British Ecological Society, UK.

Stamp, N. E. and T. M. Casey. 1993. Caterpillars: ecological and evolutionary constraints on foraging. . Chapman & Hall, New York, New York, USA.

Strong, D., J. H. Lawton, and T. R. E. Southwood. 1984. Insects on Plants: community Patterns and Mechanisms. Blackwell Scientific Publications, Oxford, UK.

Sudhira, H. S., T. V. Ramachandra, A Wytzisk, and C. Jeganathan. 2005. Framework for Integration of Agent-based and Cellular Automata Models for Dynamic Geospatial Simulations.*in* Centre for Ecological Science, editor., Bangalore, India.

Sun, G. Q., Z. Jin, Q. X. Liu, and L. Li. 2008. Chaos induced by breakup of waves in a spatial epidemic model with nonlinear incidence rate. Journal of Statistical Mechanics-Theory and Experiment.

Taylor, C. M. and A. Hastings. 2005. Allee effect in biological invasions. Ecological Letters 8:895-908.

Tisdale, S. L., W. L. Nelson, and J. D. Beaton. 1985. Soil Fertility and Fertilizers. Macmillan Publishing Company, New York, New York, USA.

Tollrian, R. and C. D. Harvell. 1998. Ecology and Evolution of Inducible Defenses. Princeton University Press, Princeton, NJ, USA

USFS. 2011. Birch Leaf Miners. Forest Health Conditions in Alaska 2011. A Forest Health Conditions Report. Accessed on October 25, 2012. http://www.fs.usda.gov/Internet/FSE_DOCUMENTS/stelprdb5360665.pdf,

Varley, G., G. R. Gradwell, and M. P. Hassell. 1973. Insect Population Ecology. University of California Press, Berkeley, California, USA.

von Neumann, J. 1951. The General and Logical Theory of Automata. Pergamon Press, London, UK.

Yemshanov, D., F. H. Koch, D. W. McKenney, M. C. Downing, and F. Sapio. 2009. Mapping Invasive Species Risks with Stochastic Models: A Cross-Border United States-Canada Application for Sirex noctilio Fabricius. Risk Analysis 29:868-884.

Ylioja, T., H. Roininen, M. P. Ayres, M. Rousi, and P. W. Price. 1999. Host-driven population dynamics in an herbivorous insect. . Proceeding National Academe Science 96:10735-10740.

Zhou, G. F. and A. M. Liebhold. 1995. Forecasting the spatial dynamics of gypsy-moth outbreaks using cellular transition models. Landscape Ecology 10:177-189.

APPENDIX 1

```
# Simulation model of P. thomsoni severity
#
library(RandomFields)
Itr <- 100
Yrs<-14

#function to generate spatially correlated surfaces
#
surface<-function(x,y,model,mean,variane,nugget,scale,alpha,graph.I=F,graph.P=F,g.title="") {
out<- GaussRF(x=x, y=y, model=model, grid=TRUE,param=c(mean, variance, nugget, scale,
alpha))
if(graph.I) {
windows()
image(x, y, out)
contour(x,y,out,add=T)
title(g.title)
}
if(graph.P) {
windows()
persp(x,y,out, theta = -35,phi = 20,expand = 0.7,col = "lightblue",ltheta = 150, shade =
0.55,ticktype ="detailed",xlab ="X",ylab = "Y",zlab = "Density",cex=.5)
title(g.title)
}
out
}

#loop through simulations
#
for( i in 1:Itr) {
cat("\n Itr = ",i)

#predicted 06

 model <- "matern"
 mean <- -0.1121
 variance <-  3
 nugget <- 0
 scale <- 3685
 alpha <- 3
 step <- 1000
 x <- seq(1641272, 1685601, step)
 y <- seq(2591899, 2642359, step)
g.title<-"Predicted 06"
f06 <- surface(x=x,y=y,model=model,mean, variance, nugget, scale,
alpha,graph.I=F,graph.P=F,g.title)

#add mean
```

```
mu<-26.9
f06<-f06+mu

#create new data set

ablm.old<-list(x=x,y=y,z=f06)

#set negative values to 0

ablm.old$z[ablm.old$z<0]<-0
mu06<-mean(as.vector(ablm.old$z))

#plot trimmed surface

if(i ==1) {

windows()
persp(ablm.old, theta = -35,phi = 20,expand = 0.7,col = "lightblue",ltheta = 150, shade =
0.55,ticktype ="detailed",xlab ="X",ylab = "Y",zlab = "Density",cex=.5)
title("Predicted 06 - Trimmed")
}

nc<-ncol(f06)
nr<-nrow(f06)
delta0<-matrix(0,nrow=nr,ncol=nc)
delta.cum<-delta0
stat<-mu06

#simulate the time periods

for(j in 1:Yrs) {

############################
#generate areas of random size and shape 10% to 50% of area
# mean = 0 range = 3685 feet, variance = 1
model <- "matern"
mean <- 0
 variance <- 1
 nugget <- 0
 scale <- 3685
 alpha <- 6
 step <- 1000
 x <- seq(1641272, 1685601, step)
 y <- seq(2591899, 2642359, step)
g.title<-"Random Blob"
delta1<- surface(x=x,y=y,model=model,mean, variance, nugget, scale,
alpha,graph.I=F,graph.P=F,g.title)
delta1s<-delta1

rnd<-runif(1,min=0.10,max=0.5)
zcut<-1.49-2.78*rnd
```

```
zcut.sub<-zcut*1.85

delta1[delta1>zcut]<-1
delta1[delta1!=1]<-0

#create subset

delta1s[delta1s>zcut.sub]<-1
delta1s[delta1s!=1]<-0


#create new data set

#set excess overlap to zero

delta1<-(1-delta0)*(delta1-delta1s)+delta1s

#calculate cumulative area

delta.cum<-delta.cum+delta1
delta.cum[delta.cum>1]<-1


if(i == 1) {
}

################################
#change model

#random error
model <- "matern"
mean <- 0
variance <- 4
nugget <- 0
scale <- 3685
alpha <- 3
step <- 1000
x <- seq(1641272, 1685601, step)
y <- seq(2591899, 2642359, step)
g.title<-"Random Error"
fd<- surface(x=x,y=y,model=model,mean, variance, nugget, scale,
alpha,graph.I=F,graph.P=F,g.title)


# trend surface
# log model
b0<- -4.538418943+1.532291784*log(j)
b02<- 17.04998835-2.930385669*log(j)
b2<- b02-b0
#cos model
b1<- (-0.255196006-0.142286324*cos(j-3))
```

```
mu<- b0+b1*ablm.old$z+b2*delta1
fd<-fd+mu

##################################
#predicted surface

#create new data set

ablm.new<-list(x=x,y=y,z=fd)

#add change to predicted 06 surface

ablm.new$z<-ablm.new$z+ablm.old$z

#set negative values to 0

ablm.new$z[ablm.new$z<0]<-0
mu.new<-mean(as.vector(ablm.new$z))

#plot trimmed surface

if(i ==1) {
windows()
persp(ablm.new, theta = -35,phi = 30,expand = 0.7,col = "lightblue",ltheta = 150, shade =
0.55,ticktype ="detailed",xlab ="X",ylab = "Y",zlab = "Density",cex=.5)
g.title<-paste("Year",j,sep=" ")
title(g.title)
}

###################################
#change stats

#means of the two groups

mu0<-mean(as.vector(ablm.new$z[delta1==0]))
mu1<-mean(as.vector(ablm.new$z[delta1==1]))
mu0.p<-mean(as.vector(ablm.old$z[delta1==0]))
mu1.p<-mean(as.vector(ablm.old$z[delta1==1]))

#calculate percent area associated with increase
#
parea<-sum(delta1)/(nrow(delta1)*ncol(delta1))
cum.area<-sum(delta.cum)/(nrow(delta1)*ncol(delta1))

#calculate overlap of two periods

delta<-delta0*delta1
parea.ovr<-sum(delta)/sum(delta1)
########################
# generate statistics to evaluate fit
```

```
stat<-cbind(stat,mu.new,mu0.p,mu0,mu1.p,mu1,parea,parea.ovr,cum.area)

delta0<-delta1
ablm.old<-ablm.new

#end year loop
}

if(i == 1) {
stat.sim<-stat
}
else {
stat.sim<-rbind(stat.sim,stat)

}

#end simulation loop
}
##########################################

cat("\n summary Statistics\n")
cat("Year 2006\n")
summary(stat.sim[,1])
lb<-2
ub<-9
inc<-8
for(j in 1:Yrs) {
cat("Year ",j,"\n")
print(summary(stat.sim[,lb:ub]))
write.table(summary(stat.sim[,lb:ub]), "c:/temp/sim_run4.txt", col.name=T, row.name=T,
append=T, sep="\t")
lb<-ub+1
ub<-ub+inc
}
k<-8*Yrs+1
id<-seq(2,k,8)
windows()
par(mfrow=c(2,2))
hist(stat.sim[,1],main="Year 2006",xlab="Severity")
abline(v=mean(stat.sim[,1]),col=2,lwd=2)
j<-4
for(i in 1:Yrs) {
if(i == j) {
windows()
par(mfrow=c(2,2))
j<-j+4
}
h.title<-paste("Year",i,sep=" ")
hist(stat.sim[,id[i]],main=h.title,xlab="Severity")
abline(v=mean(stat.sim[,id[i]]),col=2,lwd=2)
}
```